國 立 交 通 大 學

照明與能源光電研究所

碩 士 論 文

金屬環雷射之熱特性

Thermal Properties of Metal Ring Laser

研 究 生 ： 陳彥中

指導教授 ： 施閔雄 教授

林俊廷 教授

中華民國一百零一年九月

金屬環雷射之熱特性

Thermal Properties of Metal Ring Laser

研 究 生：陳彥中　　Student：Yan-Zhong Chen

指導教授：施閔雄　　Advisor：Prof. Min-Hsiung Shih

林俊廷　　Prof. Chun-Ting Lin

國 立 交 通 大 學

照明與能源光電研究所

碩 士 論 文

A Thesis

Submitted to Institute of Lighting and Energy Photonics

College of Photonics

National Chiao Tung University

in partial Fulfillment of the Requirements

for the Degree of

Master in

Lighting and Energy Photonics

September 2012

Tainan, Taiwan, Republic of China

中華民國一百零一年九月

金屬環雷射之熱特性

研究生：陳彥中　　指導教授：施閔雄教授
林俊廷教授

國立交通大學照明與能源光電研究所碩士班

摘要

本論文中，我們直接接合方式將半導體材料接合在雙面拋光的藍寶石基板上，藍寶石基板有良好的導熱性外，再近紅外光也有良好的透光性和低折射率，適合在覆蓋金屬後，利用從藍寶石基板端注入能量和接收訊號的方式，解決金屬吸收大而難以接收訊號的問題。並且用模擬的方式來分析實驗結果。接著，我們用簡單的利用量測的方式，利用改變溫度及注入的能量來改變雷射波長，獲得熱阻值，也證實了當覆蓋金屬後，熱大部分都是藉由金屬層傳導。

Thermal Properties of Metal Ring Laser

Student : Yan-Zhong Chen Advisor: Prof. Min-Hsiung Shih
Prof. Chun-Ting Lin

Institute of Lighting and Energy Photonics
National Chiao Tung University

Abstract

In the thesis, the InGaAsP use wafer bonding on double polish sapphire. The sapphire has high thermal conductivity, low index and high transmission in NIR. We can use input power and accept sign for sapphire after coating metal. In order to solve the metal has high absorption that the sign is different accept if pumping from metal. And simulation used to compete with the measurement result. Next part, thermal resistance was estimated by measuring lasing wavelength shifting with temperature and pumping power variation individually. The major parts heat flux is contact by metal layer when coating metal.

Acknowledgement

研究所兩年的時間說長不長，說短不短，這些日子來感謝實驗室裡的每個人，感謝老師這兩年來不管是在研究上，甚至在教育上都給了很多建議，也感謝老師在最後口試時給很許多意見及幫助，這兩年的教導會謹記在心。感謝功書學長在最後量測、數據分析上給了許多的幫助。感謝怡君、旻彥學姐在量測及模擬上給了許多的建議，讓我能快速的上手。感謝子庭學長從 SEM training，到 E-beam、Wet Bench、ICP training，除了他自己的研究進度，還抽出時間training，讓我趕快的上手。感謝坤廷這兩年的陪伴，同為南交的學生，不管在課業上還是研究上，都給了許多的幫助。感謝志祺最後幾個月在量測給了許多的幫助。感謝昭瑋、湘諭平時的照顧。感謝祥鳴、祥宇、柏霈、瑋彬學弟們平日的相處，尤其是祥鳴跟柏霈有事沒事就跟你們發牢騷。感謝南交大的大家及球隊的各位平時照顧。最後感謝我的家人給了我許多的幫助及支持，能讓我專心地完成我的學業。

Content

摘要..... I

Abstract..... II

Acknowledgement..... III

Content..... IV

List of Figures..... VI

List of Tables..... XI

Chapter 1 Introduction

1-1 Semiconductor laser..... 1

1-2 Plasmonic..... 3

1-3 Plasmonic Laser..... 5

1-4 Thermal Conductivity..... 7

1-5 Motivation..... 10

Chapter 2 Fabrication Process

2-1 Introduction..... 11

2-2 Fabrication steps for plasmonic laser on sapphire..... 11

2-2-1 Direct Wafer Bonding Process..... 17

2-2-2 E-Beam Lithography..... 20

2-2-3 Inductively Coupled Plasma Reactive Ion Etching..... 21

2-2-4 Thermal Coater 23
2-3 Conclusion 24

Chapter 3 Nano-Ring Laser Cavity on Sapphire

3-1 The Micro-PL Measurement System 25
3-2 Nano-Ring Laser on Sapphire 27
3-3 Metal Nano-Ring Laser on Sapphire at 80K 32
3-4 Simulation 37
3-5 Conclusion 43

Chapter 4 Thermal Properties of Gold-Coating Ring on Sapphire

4-1 Temperature-Dependent Lasing Wavelength 44
4-2 Pumping Power-Dependent Lasing Wavelength 52
4-3 Thermal resistance of Gold-Coating Ring 56
4-4 Conclusion 59

Chapter 5 Conclusion and Outlook

References

Appendix

List of Figures

Figure 1-1 1 Some of the laser applications (a) Optics storage. (b) Medicine. (c) Industry. (d) Communication 1

Figure 1-1 2 Micro- and nano-laser (a) VCSEL. (b) Microdisk. (c) Photonic crystal 2

Figure 1-2 1 (a) A surface plasmon polaritions propagate at the interface and (b) A localized surface plasmon of spherical metal particles oscillating with the electromagnetic field 4

Figure 1-4 1 The heat fluxes distribution that (a) and (b) are suspend membrane D3 cavity. Then (c) and (d) are D3 cavity on sapphire 8

Figure 2-2 1 The epitaxial structure of InGaAsP MQWs 12

Figure 2-2 2 The fabrication process of the plasmonic laser on the sapphire substrate 16

Figure 2-2 3 The SEM image is plasmonic laser device on sapphire form top view 16

Figure 2-2 4 The curve of anneal temperature with anneal time 18

Figure 2-2 5 (a) and (b) are InGaAsP bonded on sapphire sample after etching. Viewing of (a)is form InGaAsP and (b) is form sapphire 19

Figure 2-2 6 The annealing system is used in the bonding process 19

Figure 2-2 7 The nano-scale patterns obtained through the SEM/E-beam system 20

Figure 2-2 8 The ICP-RIE system is used for dry etching..... 22

Figure 2-2 9 Angle view of SEM image after InP etching..... 22

Figure 2-2 10 SEM image is InGaAsP cavity coating Gold. (a) Top view and (b) angle view of the plasmonic laser cavity..... 23

Figure 3-1 1 The picture of micro-PL measurement system..... 25

Figure 3-2 1 SEM image of the nano-ring cavity. Its diameter is 4 μm, and width is 420 nm. (a) Top view and (b) (c) angle view of the nano-ring cavity..... 27

Figure 3-2 2 The PL pumped from air side is black line and pumped from sapphire side is red line..... 28

Figure 3-2 3 (a) Air-InGaAsP-Air and (b) Air-InGaAsP-Sapphire optical leak distributions..... 29

Figure 3-2 4 The sapphire the transmission spectrum in NIR..... 29

Figure 3-2 5 The black line is pumped from air side, that lasing wavelength is about 1508.2 nm. The red line is pumped from sapphire side, that lasing wavelength is about 1507.5 nm..... 30

Figure 3-2 6 The threshold power are 13 mW and 12.5 mW each of pumped from air side and sapphire side..... 31

Figure 3-3 1 SEM image of the coated gold nano-ring cavity. The thickness of gold is about 200 nm. (a) Top view and (b) (c) angle view of the nano-ring cavity..... 32

Figure 3-3 2 The sample is putted in the crystate..... 33

Figure 3-3 3 The sample is after coating gold. Viewing of (a) is from gold and (b) is from sapphire 33

Figure 3-3 4 The PL pumped without gold from sapphire is black line, pumped from gold is red line, and pumped from sapphire is blue line 34

Figure 3-3 5 Reflection of gold in NIR..... 35

Figure 3-3 6 Transmission of gold in NIR 35

Figure 3-3 7 (a) The lasing wavelength are 1475.2 nm for non-coating ring, and 1311 nm for ring gold-coating ring. (b) The threshold power are 1.3 mW for non-coating, and 8 mW for ring gold-coating. 36

Figure 3-4. 1 The simulation diagram. (a) is non-coating ring on sapphire and (b) is gold-coating ring on sapphire 37

Figure 3-4 2 The normalize H field of the non-coating ring. (a) top view (b) side view..... 38

Figure 3-4 3 The measurement compares with simulation result. The lasing wavelength is 1478.9 nm and quality factor about 12300 for measurement. The wavelength is 1470 nm and quality factor about 1000 for simulation..... 39

Figure 3-4 4 The normalize of H field. (a) top view (b) side view 40

Figure 3-4 5 The measurement compares with simulation result. The lasing wavelength is 1311 nm and quality factor about 3700 for measurement. The wavelength is 1300 nm and quality factor about 400 for simulation..... 41

Figure 3-4 6 (a) The mode profile of total energy. (b) The distribution of energy 42

Figure 3-4 7 (a) The mode profile of total energy. (b) The distribution of energy 42

Figure 4-1 1 The PL wavelength shifts with temperature variation of the ring (a) non-coating and (b) gold-coating..... 45

Figure 4-1 2 The PL wavelength shifts with temperature variation of the non-coating is black point and gold-coating is red point. (a) is peak 1 that the $\Delta\lambda/\Delta T$ are 0.46 nm/K non-coating and 0.48 nm/K gold-coating. (b) is peak 2 that the $\Delta\lambda/\Delta T$ are 0.57 nm/K non-coating and 0.53 nm/K gold-coating 46

Figure 4-1 3 The lasing wavelength shifts with temperature variation for non-coating ring. The temperature changes from 80K to 300K. The lasing wavelength is from 1492 nm to 1507 nm..... 47

Figure 4-1 4 The lasing wavelength shifts with temperature variation. The temperature changes from 80K to 300K, and $\Delta\lambda/\Delta T$ is 0.063 nm/K 48

Figure 4-1 5 The lasing wavelength shifts with temperature variation. The temperature changes from 80K to 150K. The lasing wavelength is from 1311 nm to 1313 nm. 49

Figure 4-1 6 The lasing wavelength shifts with temperature variation. The temperature changes from 80K to 140K, and $\Delta\lambda/\Delta T$ is 0.026 nm/K 50

Figure 4-1 7 The lasing wavelength shifts with temperature variation. The measurement compares with simulation of the ring (a) non-coating and (b) gold-coating..... 51

Figure 4-2 1 The lasing wavelength shifts with pumping power variation. (a) The Δλ/ΔP is 0.151 (nm/mW) of the non-coating ring. (b) The Δλ/ΔP is -0.052 (nm/mW) of gold-coating ring 52

Figure 4-2 2 The non-coating ring on sapphire (a) 3-D view (b) top view..... 54

Figure 4-2 3 The gold-coating ring on sapphire (a) 3-D view (b) top 54

Figure 4-2 4 The heat fluxes distribution for non-coating ring on sapphire (a) top view and (b) side view. The highest temperature is 380K. The major of heat heats are through sapphire layer. And the heat fluxes distribution for gold-coating ring on sapphire (c) top view and (d) side view. The highest temperature is 330K. The major of heat heats are through gold layer, secondary through sapphire layer..... 55

Figure 4-3 1 The non-coating ring on sapphire. The Δλ/ΔT is about 0.063 (nm/K), and the Δλ/ΔP is about 0.151 (nm/mW)..... 57

Figure 4-3 2 The gold-coating ring on sapphire. The slope Δλ/ΔT is about 0.028 (nm/K), and the slope Δλ/ΔP is about -0.052 (nm/mW) 57

Figure 4-3 3 With simulation to estimate ΔT/(ΔP)that black points are 80 K/mW for non-coating ring, and red points 33 K/mW for gold-coating ring .. 58

Figure A-1 The non-coating ring on sapphire. The Δλ/ΔT is 0.048 (nm/K), and the Δλ/ΔP is 0.142 (nm/mW) 68

Figure A-2 The non-coating ring on sapphire. The Δλ/ΔT is 0.021 (nm/K), and the Δλ/ΔP is -0.029 (nm/mW)..... 68

List of Tables

Table 1-3 1 The some research results of plasmonic laser around the world in recent years. 6

Table 4-2 1 The simulation parameters 53

Table 4-3 1 The thermal resistance compares measurement with simulation..... 58

Table A 1 The thermal resistance compares measurement with simulation at CW pumping condition 69

Chapter 1 Introduction

1-1 Semiconductor laser

The first Ⅲ-Ⅴ semiconductor laser had been invented by Robert N. Hall. Since then, scientists had developed the semiconductor laser in the whole world, and more diversified in the application, such as optics storage [1], medicine [2], industry [3] and communication [4].

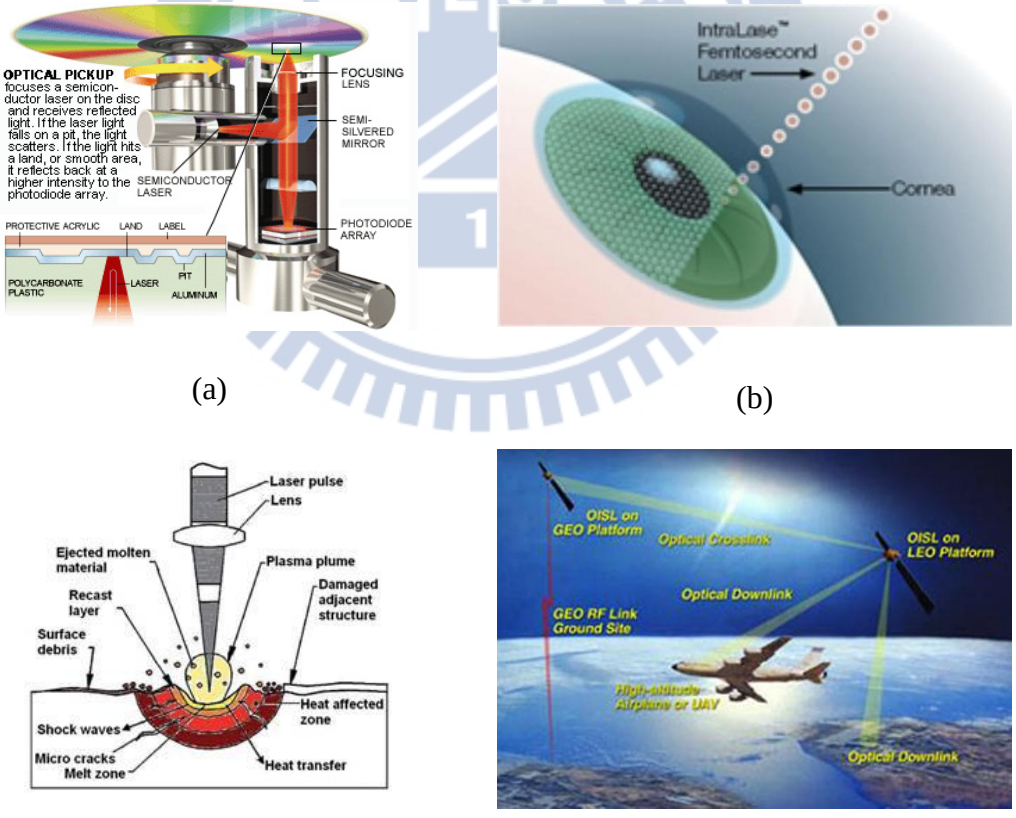

(a) (b)

(c) (d)

Figure 1-1 1 Some of the laser applications (a) Optics storage [1]. (b) Medicine [2]. (c) Industry [3]. (d) Communication [4].

In recent year, the semiconductor laser diameter more and more small with the technical advance, such as VCSEL [5] microdisk [6], photonic crystal [7,8]. But limit of physics with the shrinking dimension. The smallest dimensions to which the optical mode of such cavities can be confined is related to the diffraction limit , and is of the order of one half of the wavelength of light in the dielectric material [9]. The metal cans as a strong mirrors, that optical mode is allowed smaller than the diffraction limit. The light is confined at the interface between metal and dielectric that is called surface plasmon polaritons (SPPs). The laser cavity size is shrunk than the wavelength of light, which is reduced below the diffraction limit to the optical mode dimension. When laser size is shrunk, which the other factor is more important that is thermal conductivity. The laser size is shrunk, and the area of heat fluxes is decrease, too.

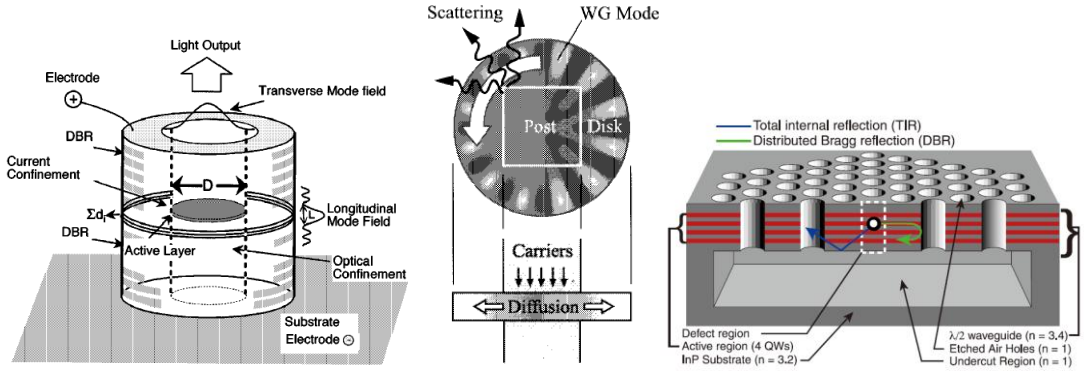

(a) (b) (c)

Figure 1-1 2 Micro- and nano-laser (a) VCSEL [5]. (b) Microdisk [6]. (c) Photonic crystal [8].

1-2 Plasmonic

The plasmons lasers have use two types surface plasmon polariton and localized surface plasmons [10]. Surface plasmons (SPs), a near-field phenomenon of surface electron oscillations, originate from the interactions between incident electromagnetic (EM) field and free electron in metal [11,12].SPs have lower energy which quantize the longitudinal electron oscillations about positive ion cores within the bulk of an electron gas. The other is localized surface plasmons, is non-propagating excitations of the conduction electrons of metallic nanoparticles coupled to the electromagnetic field. Figure 1-2 1 shows surface plasomn polarition and localized surface plasmon diagram.

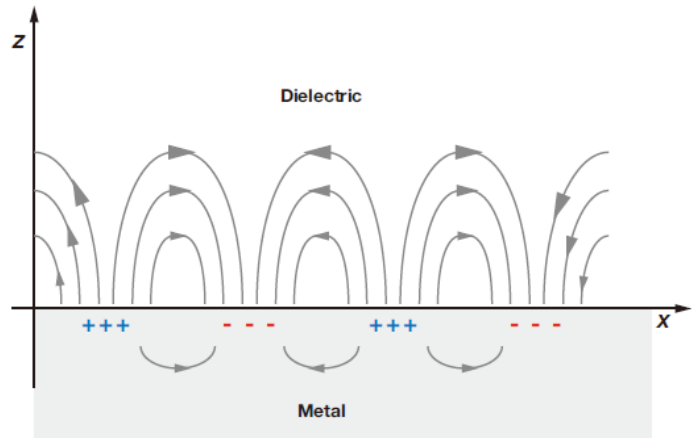

(a)

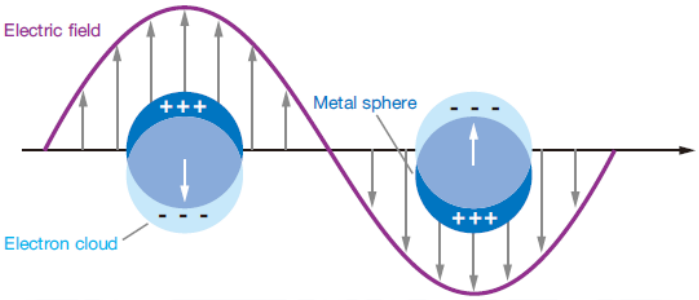

(b)

Figure 1-2 1 (a) A surface plasmon polaritions propagate at the interface and (b) A localized surface plasmon of spherical metal particles oscillating with the electromagnetic field [13].

1-3 Plasmonic Laser

Recently, the plasmonic laser has been important direction in the world, which except the metal has high absorption and high loss in subwavelength. The advantages of coating metal can further shrink lasing cavity diameter, high reflection in subwavelength, and high thermal conductivity. Many of researches have been proposed in the past few years.

The first of demonstrated metal laser is M.T. Hill *et al* [14]. They coated Ag and dielectric layer on the nanorod that use electrically pumped at 77K in 2007. The nanorod size is 200~300 nm, the lasing wavelength is 1435 nm. After then they designed different metal laser cavities such as the metal-insulator-metal (MIM) waveguide structure in 2009 [15]. The lasing wavelength is 1510 nm at room temperature. And the plasmonic distributed feedback (DFB) laser use electrically pumped at room temperature in 2011 [16] that has been proved which confine light to below the diffraction limit. Then M. W. Kim *et al* demonstrated a metal-clad semiconductor nanoring laser [17-19]. Even the metal structure has been applied to nanobeam cavity example A. M. Lakhani *et al* [20] and X. Yang *et al* [21]. Above, they applied communication and infrared wavelengths. Y. G. Wang *et al* applied ultraviolet region that aluminum coating GaN nanocavity at room temperature [22.23].

Table 1-3 1 shows some research results of plasmonic laser around the world in recent years.

M. T. Hill *et al.*	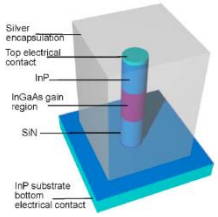 [14]	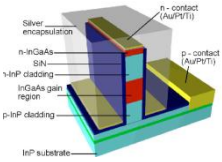 [15]	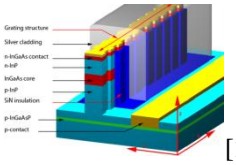 [16]
M.W. Kim *et al.*	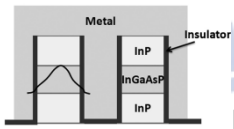 [18]		
A. M. Lakhani *et al.*	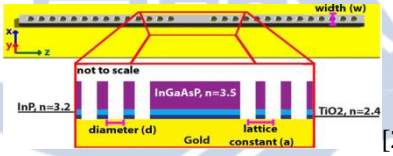 [20]		
X.Yang *et al.*	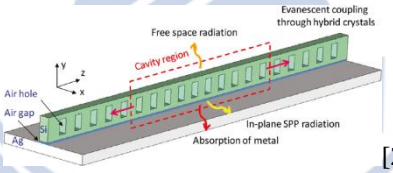 [21]		
Y. G. Wang *et al.*	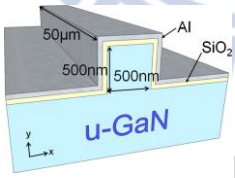 [22]	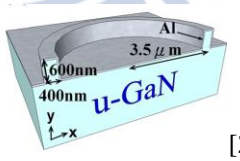 [23]	

Table 1-3 1 The some research results of plasmonic laser around the world in recent years.

1-4 Thermal Conductivity

Other limiting factor of nano-lasers is heating. The laser will bring heat when injecting energy. The heat is confined to shrinking dimensions of the laser cavity, because of the dielectric or semiconductor material has poor thermal conductivity [24], which is easy to cause of shut down. Someone want to use metal advantage of greater thermal conductivity. Such as the gold thermal conductivity is 332 (W/m-K) [25], but InGaAsP thermal conductivity only 4.2 (W/m-K) [26] and the air is 0.026 (W/m-K) [26]. So the laser size has shrunk that the heat will not easy conduct by InGaAsP or air.

Thermal conduction is one of thermal transfer types. The thermal transfer is mean a material to other material have temperature difference that cans use conduction, convection, or thermal radiation. Thermal convection is the heat from one place to another by the movement of fluids. The thermal radiation is electromagnetic radiation generated by the thermal motion of charged particles in matter. The final is thermal conduction, the between neighbor objects if have different temperature. The thermal conduction nature occurs, which no matter is solid, liquid or gas [27].

The nano-laser cavity that the major of heat transfer types is conduction. The contact will affect heat transfer rate. The substrate is one of main selects. Such as sapphire that thermal conductivity is 50(W/m-K) [28]. The sapphire as substrate has been researched [28-31]. The InGaAsP is bonded on sapphire, which the cavity is made at InGaAsP. It uses measurement and simulation to evidence that the main parts of heat flux are through sapphire layer, the cavity temperature is lower than conduction by air. Figure 1-4 1 shows the heat fluxes distribution that (a) and (b) are suspend membrane D3 cavity. Then (c) and (d) are D3 cavity on sapphire [18].

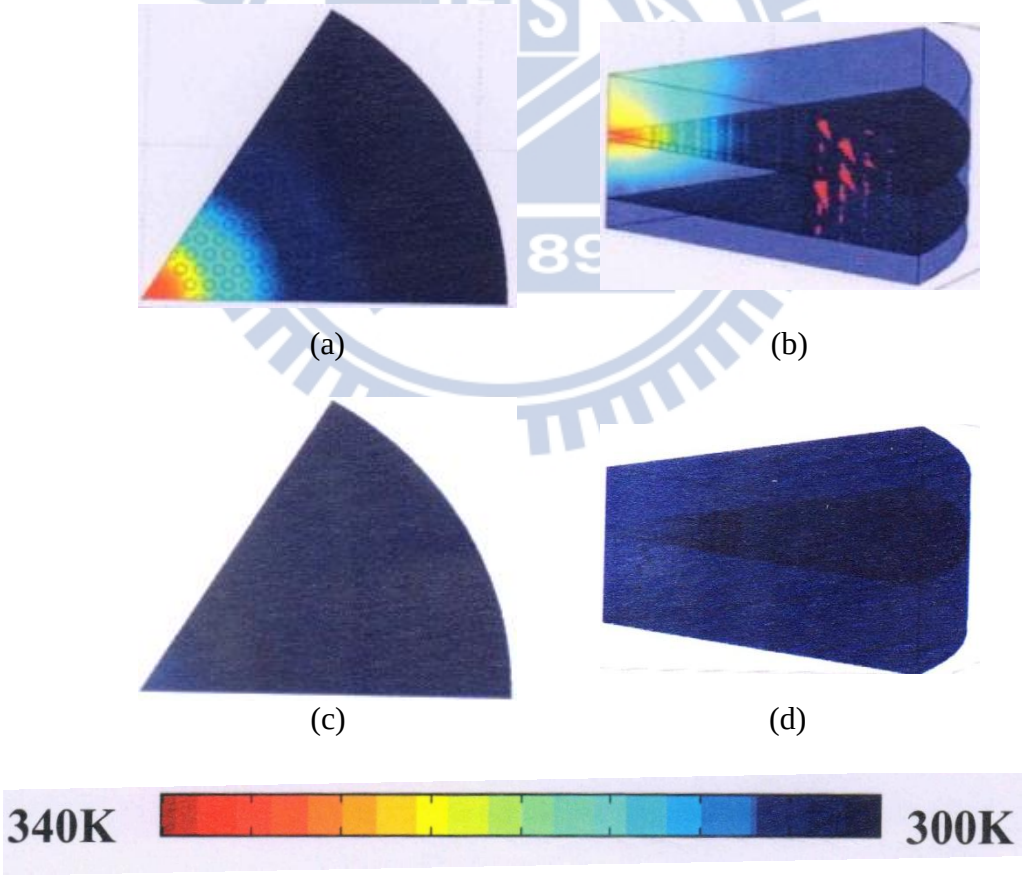

Figure 1-4 1 The heat fluxes distribution that (a) and (b) are suspend membrane D3 cavity. Then (c) and (d) are D3 cavity on sapphire [28].

At the same color bar, the sapphire of substrate that temperature is lower than with air. The major part of heat fluxes conducts through sapphire layer, but the heat fluxes are difficult through air right now. The thermal resistance is lower that cavity on sapphire than suspend membrane. It refers to use continuous wave pumping is working that the laser cavity on sapphire. In the future, it can tend to electric pumped develop that will have many application.

1-5 Motivation

Recently, the plasmonic laser is a popular research in the world. There are some advantages of using metal. The first one is reduced the size of semiconductor laser in subwavelength and high reflection. Then, the metal has good thermal conductivity then dielectric material. But the metal has high absorption that no easy accepts sign pumped from metal.

In the thesis, we use simple cavity make on the double polish sapphire and coating gold on cavity. The sapphire has high thermal conductivity, low thermal resistance and high transmission in NIR. And using measurement and simulation result compare the different. Further, we discuss the thermal resistance use different temperature and different input power to change lasing wavelength that is obtained.

In the chapter 2, we introduce the fabrication process of the metal coating cavity bonded on sapphire. Then the measurement result compares with simulation result at 80K in the chapter 3. In the chapter 4, the heat resistance will use experimental method to obtain. Finally, we give a conclusion for the thesis.

Chapter 2 Fabrication Process

2-1 Introduction

In the chapter, I will introduce the fabrication process in my laser devices. It is introduced including the direct wafer bonding, E-beam lithography, ICP-RIE etching and thermal coater the fabrication of the plasmonic laser.

2-2 Fabrication steps for plasmonic laser on sapphire

First, the step of the fabrication process is direct wafer bonding. The epitaxial structure of InGaAsP/InP MQWs used for the wafer bonding process is shown in figure 2-2 1. The wafer consist of four 10 nm 0.5%~0.7% compressively-strained InGaAsP quantum walls which are separated by five 15 nm -0.2%~0.3% tensile InGaAsP barrier layers. The thickness of the active layer is 240 nm. The emission wavelength is designed for 1550nm at room temperature.

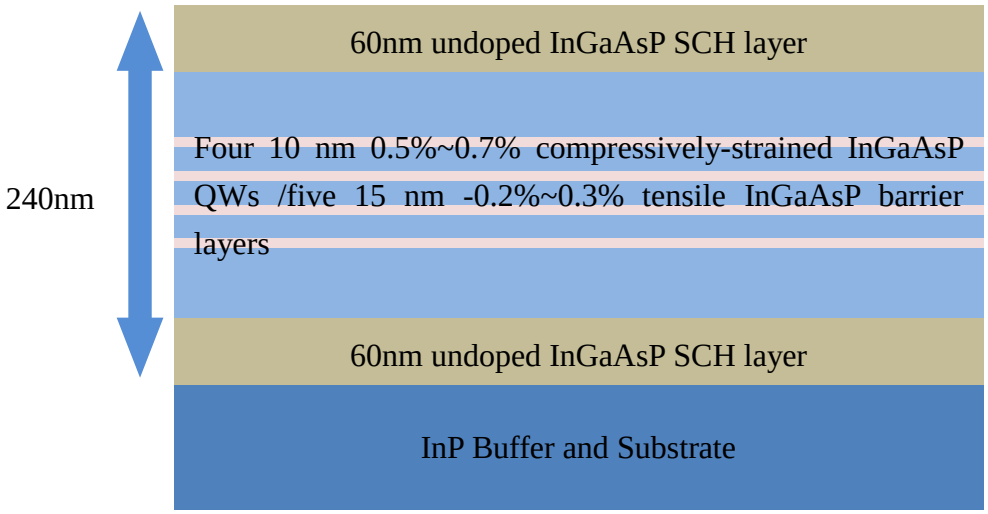

Figure 2-2 1 The epitaxial structure of InGaAsP MQWs.

The complete process of the sapphire plasmonic laser devices are shown in the figure 2-2 2. And then the introduction of bonding process, E-beam lithography, ICP-RIE and thermal coater will be discussed next.

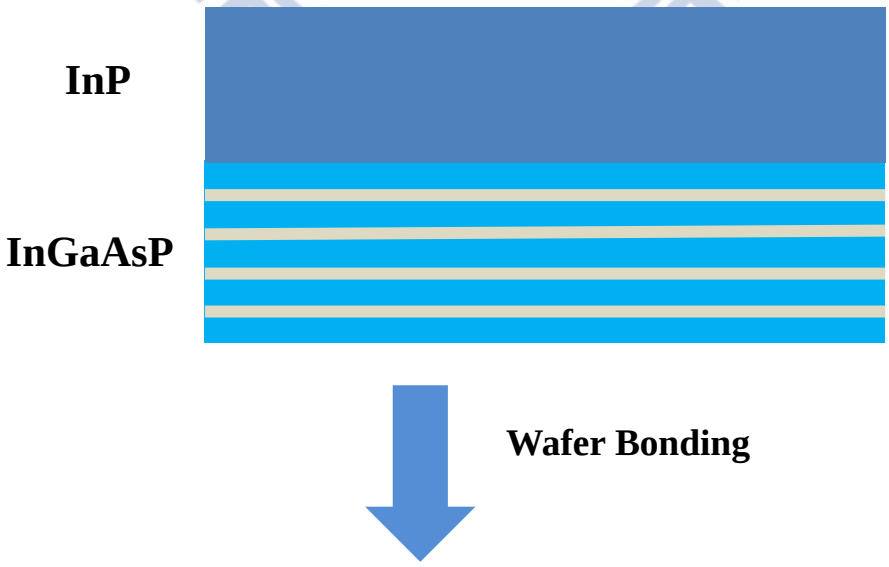

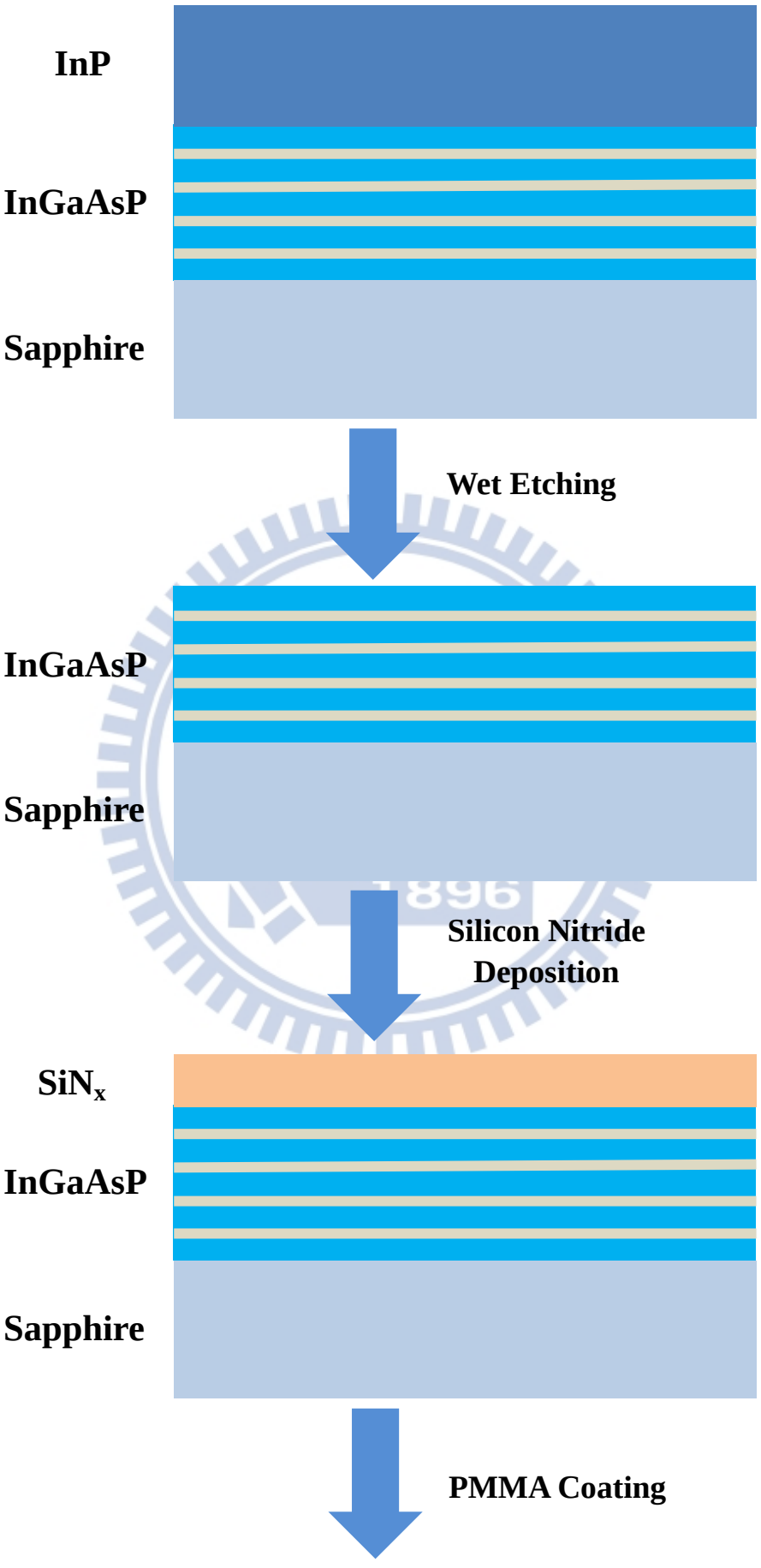
InP
InGaAsP
Sapphire
Wet Etching
InGaAsP
Sapphire
Silicon Nitride
Deposition
SiNx
InGaAsP
Sapphire
PMMA Coating

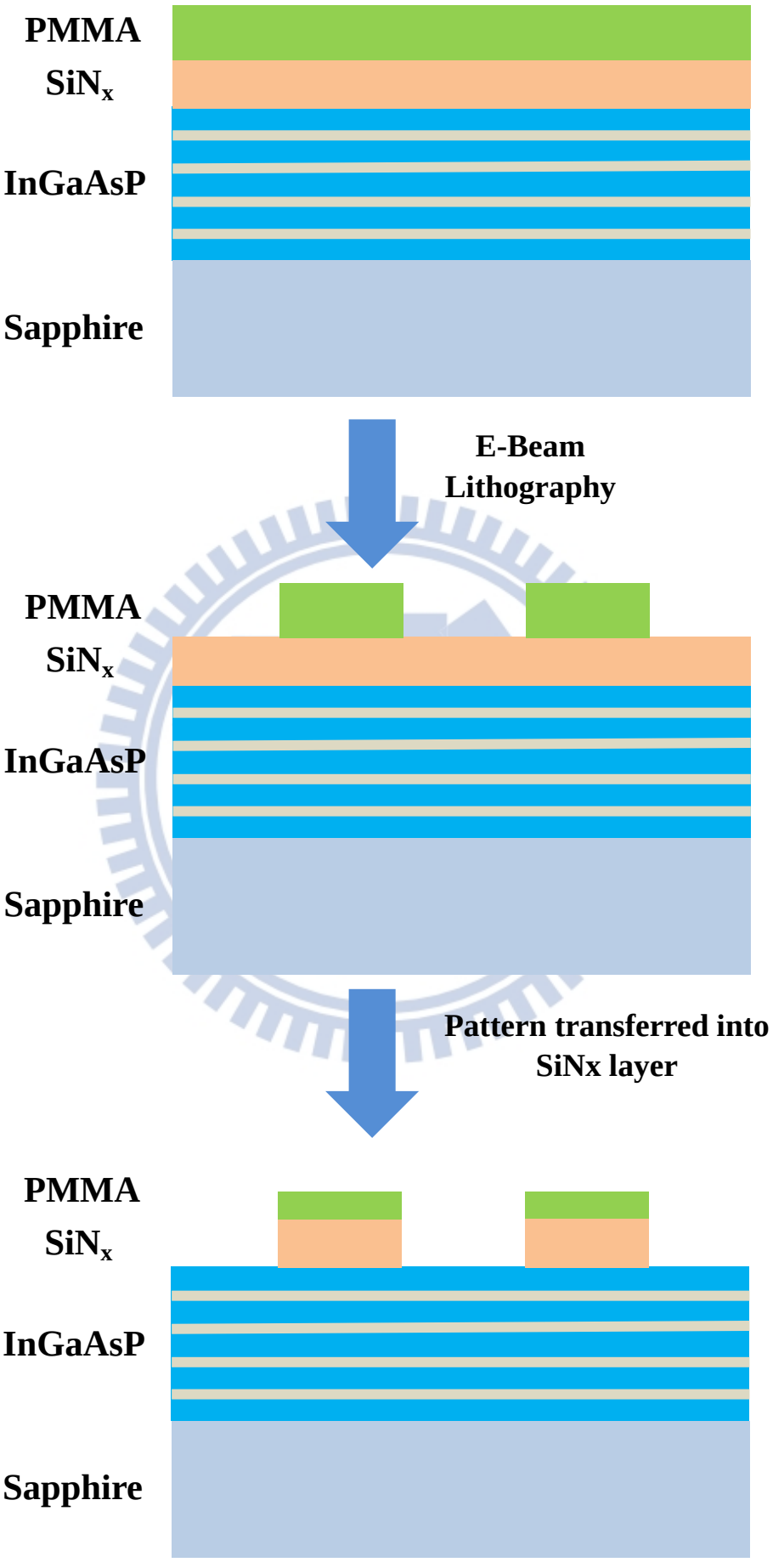
PMMA
SiNx
InGaAsP
Sapphire
E-Beam
Lithography
PMMA
SiNx
InGaAsP
Sapphire
Pattern transferred into
SiNx layer
PMMA
SiNx
InGaAsP
Sapphire

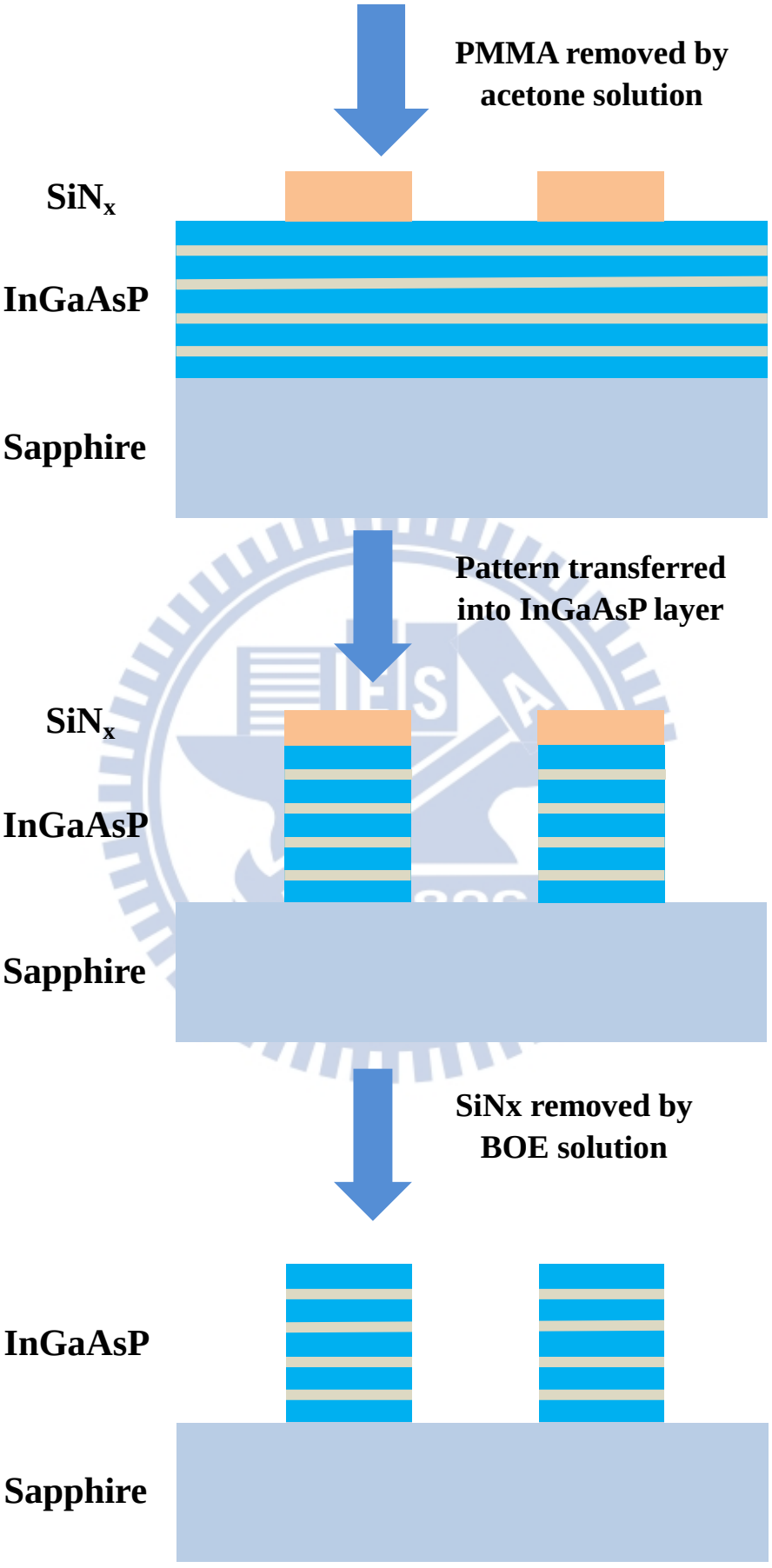
PMMA removed by
acetone solution
SiNx
InGaAsP
Sapphire
Pattern transferred
into InGaAsP layer
SiNx
InGaAsP
Sapphire
SiNx removed by
BOE solution
InGaAsP
Sapphire

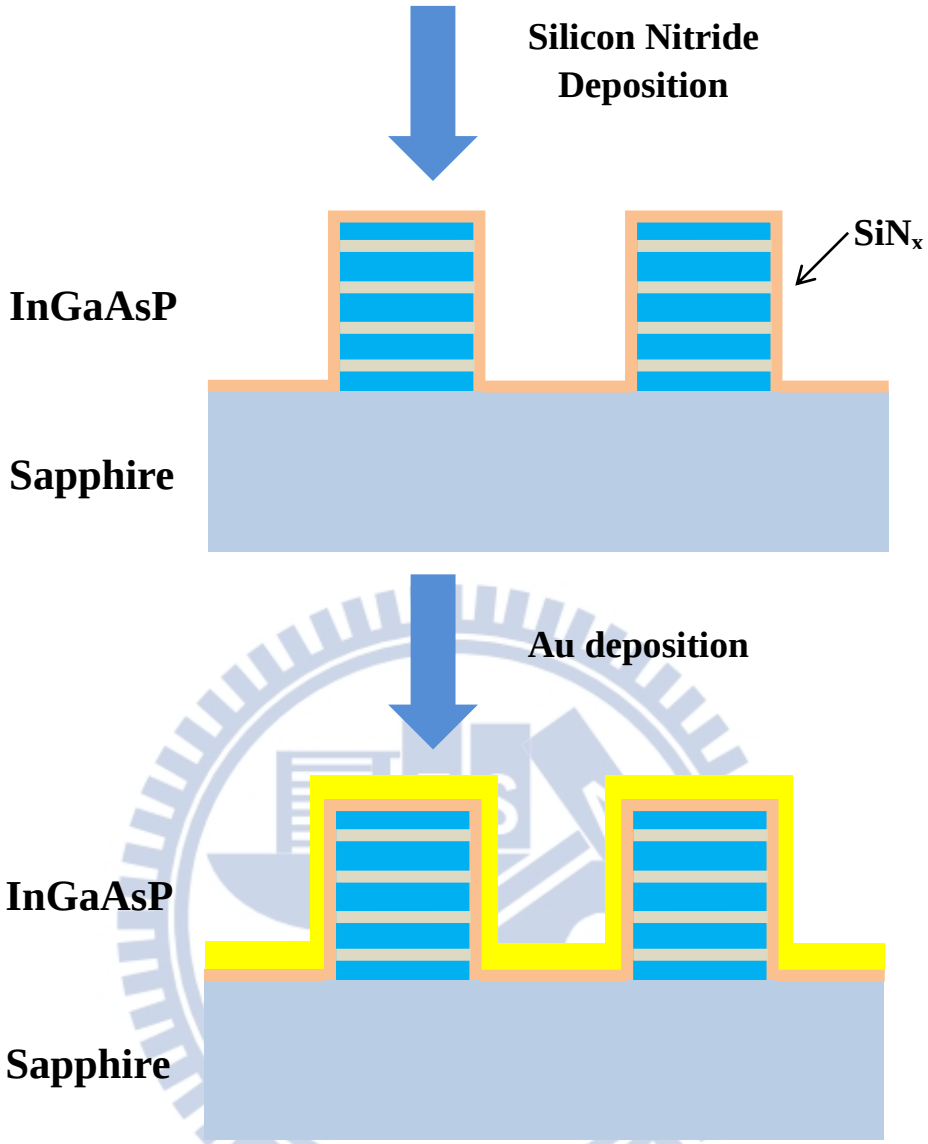

Figure 2-2 2 The fabrication process of the plasmonic laser on the sapphire substrate.

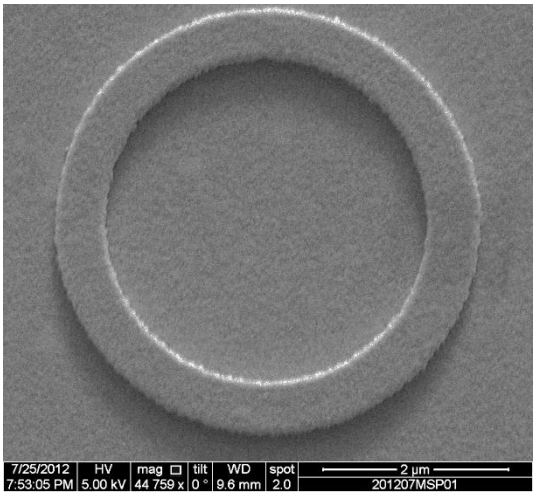

Figure 2-2 3 The SEM image is plasmonic laser device on sapphire form top view.

2-2-1 Direct Wafer Bonding Process

The first of the steps is a clean process, which are cleaned the sapphire and InGaAsP (QWs) wafer surfaces. Let particulate and organic leave for wafer surfaces. It is an important step in the fabrication process.

The sapphire wafer and InGaAsP wafer are cleaned followed by acetone, methanol, and ammonia wafer solution with ultrasonic vibration. Finally, they put in the DI wafer. After a few minutes in the DI wafer, which are bonded them face to face inside the DI wafer beaker. Move them into a graphite stage fixture and a silicon wafer put on top. Then tight the three screws on the perimeter. The steel balls are put in the screw hole at the center of the graphite stage and tight the screw in the center. It can display the torque to evaluate the pressure that is needed on the wafers and using the steel ball in the hole that provide the uniform pressure on the wafers. Then put it in the annealing chamber that is full of hydrogen.

It will have the chemical reaction to form the hydrogen bonds between sapphire and InGaAsP interface at high temperature and pressure. And use the graphite as the fixture. Its thermal expansion coefficient is low to prevent increased extra pressure and not reacting with the wafers.

The stage sets in the anneal chamber, that is heated from room temperature to 100˚C in 15 minutes and held at the temperature for 5 minutes. Let graphite stage reaches thermal equilibrium. Then heat to 480˚C in 25 minutes and held at the temperature for 60 minutes with full of hydrogen in the chamber to prevent the other gases into the chamber to form the native oxide. The nitrogen is injected into the chamber to replace the hydrogen when bonding process is finished. The figure of temperature with time in the bonding process is shown in figure 2-2 4.

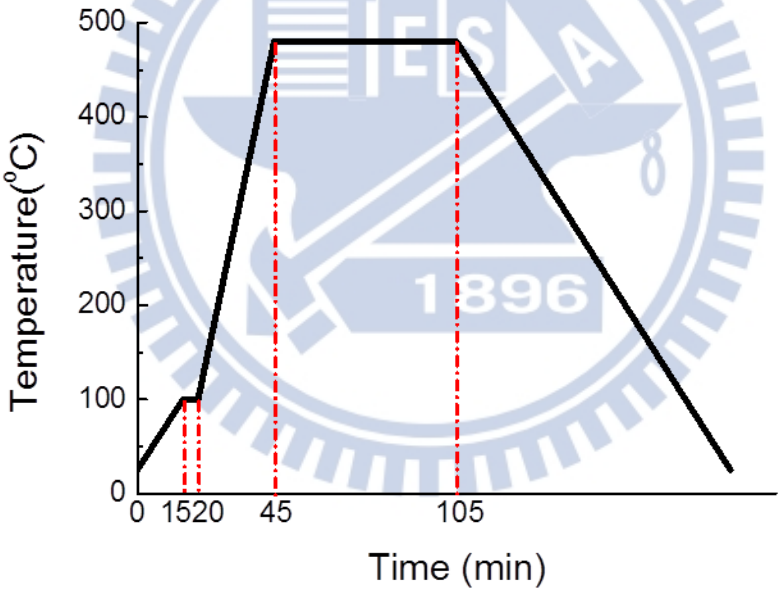

Figure 2-2 4 The curve of anneal temperature with anneal time.

When the wafer bonding is finished, with the ratio of HCl to DI water is 3:1 removing the InP substrate at room temperature. The picture is InGaAsP after wet etching which are bonded on sapphire shown in the figure 2-2 5. And figure 2-2 6 is annealing system.

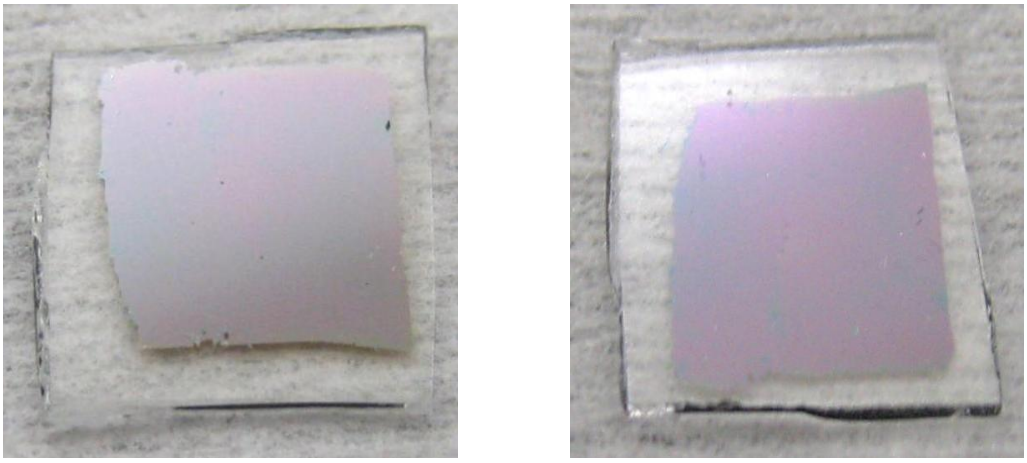

(a) (b)

Figure 2-2 5 (a) and (b) are InGaAsP bonded on sapphire sample after etching. Viewing of (a) is form InGaAsP and (b) is form sapphire.

Figure 2-2 6 The annealing system is used in the bonding process.

2-2-2 E-Beam Lithography

The next step of the process is E-beam lithography, a beam of electrons to expose the photo resist on the surface, then the patterns will be transferred to the next layer and the photo resist removed. The E-beam lithography is easy to define patterns in nano-scale. The E-beam system is showed in the figure 2-2 7.

First, we deposit the SiN_x on InGaAsP by the Plasma-enhanced chemical vapor deposition (PECVD), the photo resist Poly methyl methacrylate (PMMA) spin on the wafer by spin coater. After the patterns are defined by the E-beam system, and then developed 70 seconds by MIBK solution which the ratio of MIBK to IPA is 1:3. Putting it in IPA and in DI water remove residual IPA.

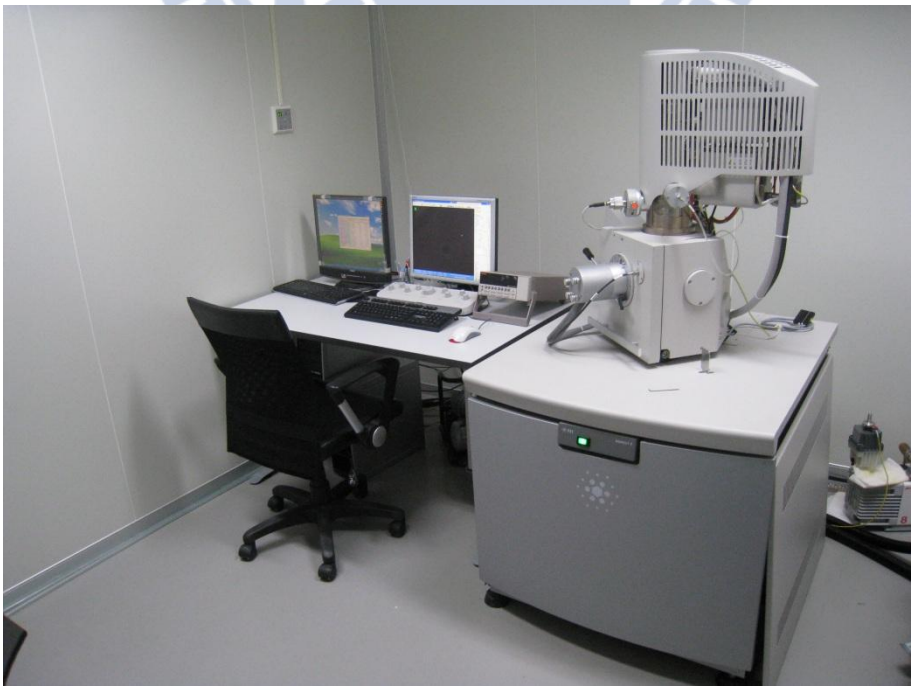

Figure 2-2 7 The nano-scale patterns obtained through the SEM/E-beam system.

2-2-3 Inductively Coupled Plasma Reactive Ion Etching

The patterns are in the nano-scale, the wet etching is no suitable. The patterns of the sidewall will be out of the besieged and line width is not easy arrive nano-scale if it uses the isotropic etching. In recent year, it replaces dry etching with dry etching in sub-micron scale in the semiconductor process. The dry etching is an anisotropic etching, which uses plasma to etch the semiconductor material. Besides, the ICP has high etching rate and cavity`s sidewall more smooth.

The ICP-RIE sysem is showed in the figure 2-2 8. The pattern is tranferred into SiN_x by the RIE with CHF_3/O_2 at 20℃. Using acetone (ACE) solution the residual PMMA layer. Then the pattern is transferred to InGaAsP quantum wall layer by the ICP with CH_4/Cl gas at 160℃. Then the SiNx layer is removed by buffer-oxide-etch (BOE). The cavity on the sapphire after the ICP etching is showed in the figure 2-2 9. The picture form the SEM, the sidewall of cavity is smooth by the ICP-RIE system.

Figure 2-2 8 The ICP-RIE system is used for dry etching.

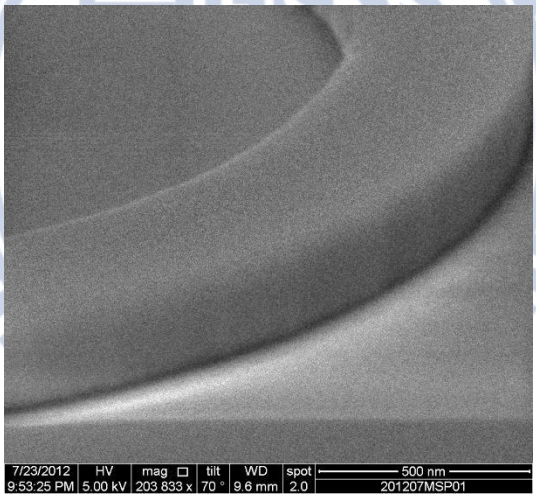

Figure 2-2 9 Angle view of SEM image after InP etching.

2-2-4 Thermal Coater

Thermal coater is one kind of physical vapor deposition (PVD). It uses resist to heat up a metal target at high vacuum, the vapor of metal will be coated on the sample surface. Before sample is coated Au, deposited SiN_x layer on the cavity surface for 30 nm. Finally, we deposit a 200nm thick gold layer with thermal coater. Figure 2-2 10 shows all of the fabrication process is finished.

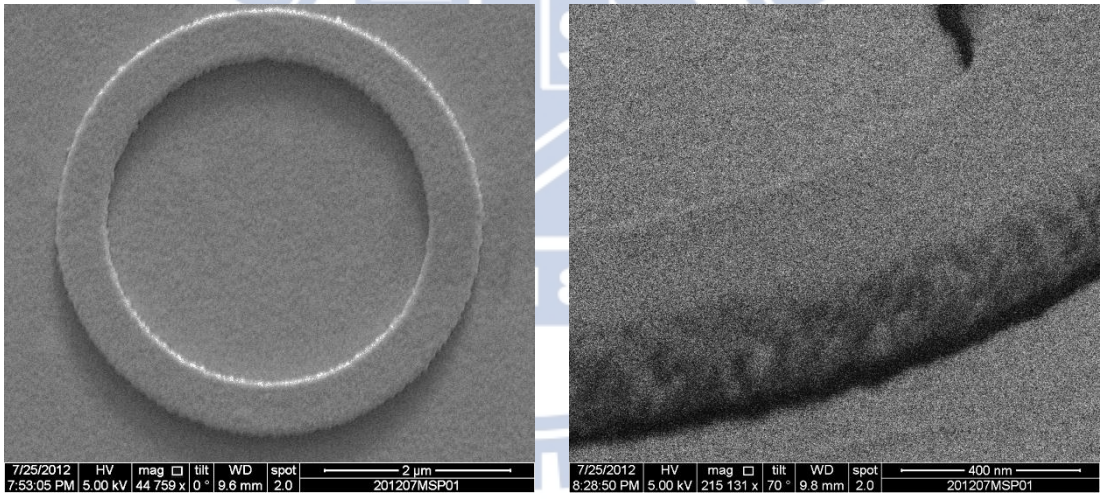

(a) (b)

Figure 2-2 10 SEM image is InGaAsP cavity coating Au. (a) Top view and (b) angle view of the plasmonic laser cavity.

2-3 Conclusion

In the chapter, the plasmonic laser has been fabricated on a sapphire substrate by wafer bonding. We also introduce the fabrication process step by step. Form wafer bonding, E-beam lithography, ICP-RIE dry etching to thermal coater. Next it will analyze the measurement with the simulation result.

Chapter 3 Nano-Ring Laser Cavity on Sapphire

In this chapter, the measurement results of the fabricated devices will be shown. The first of measurement result is compared nano-ring that pumped from InGaAsP with pumped from sapphire. Then we will compare the nano-ring coated Gold with non-coating.

3-1 The Micro-PL Measurement System

In order to measure the optical properties of the nano-ring cavities, the micro-PL measurement system with sub-micrometer scale resolution in space and sub-nanometer scale resolution in spectrum is necessary. Figure 3-1 1 shows the micro-PL measurement system.

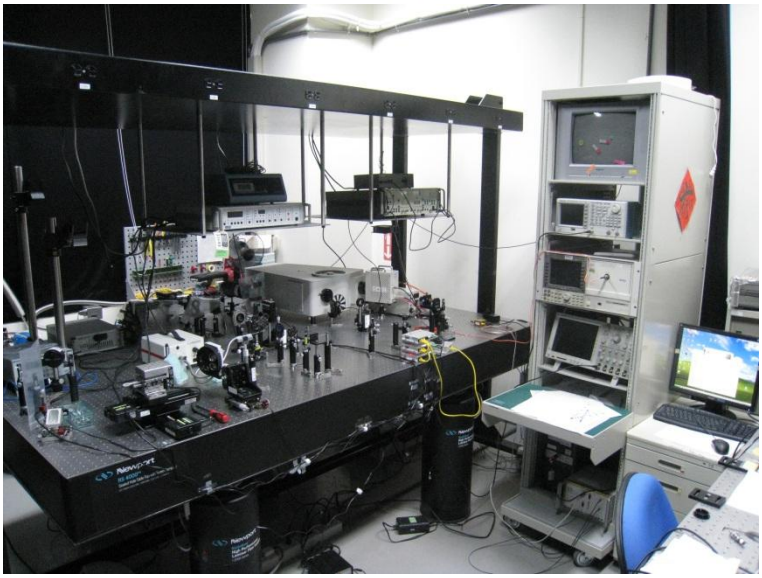

Figure 3-1 1 The picture of micro-PL measurement system.

In the measurement system, the 850 nm diode laser is used as the pump source. The pump power is modulated by the amplitude modulator, and the laser light goes through the 50/50 beam splitter, 50% of pump power is reflected into the photo-detector to know how much pump power that is used and the other 50% pump power is focused to a spot with 1.5 um to 2 μm in diameter by the 100x NIR objective lens.

The sample is mounted on a high resolution motor control 3-axis stage with 30 nm move resolution. The output power was collected from the top of the sample into the optical spectrum analyzer (OSA) by the objective lens, collective lens and multi-mode fiber. Because the nano-ring devices are only few sub-um scale, here we use the visible light system to observe the position of the pump spot and devices. The visible light system includes the visible light sources, CCD camera and monitor.

3-2 Nano-Ring Laser on Sapphire

We fabricated nano-ring on the double polishing sapphire substrate that has high transmission is can pump from sapphire. One of the fabricated nano-ring cavity is shown in figure 3-2 1. Its diameter is 4 μm, and width is 420 nm.

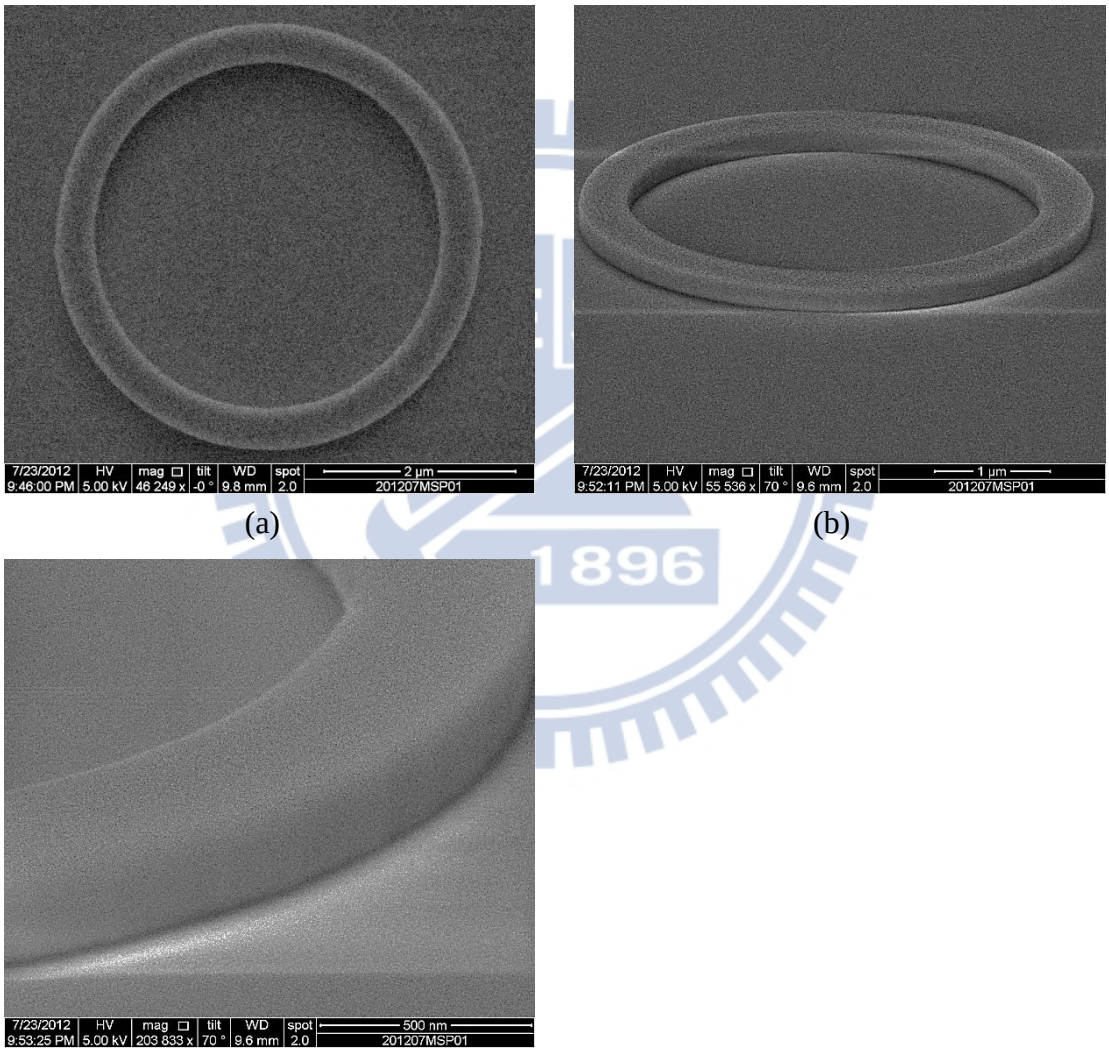

(a) (b)

(c)

Figure 3-2 1 SEM image of the nano-ring cavity. Its diameter is 4 μm, and width is 420 nm. (a) Top view and (b) (c) angle view of the nano-ring cavity.

Figure 3-2 2 shows PL pumped from air side and pumped from sapphire side. The photo-luminance spectrum (PL) of the QWs that the full-width half-maximum (FWHM) is about 200 nm. The PL is centered at 1530 nm pumped from InGaAsP and 1535nm pumped from sapphire at room temperature.

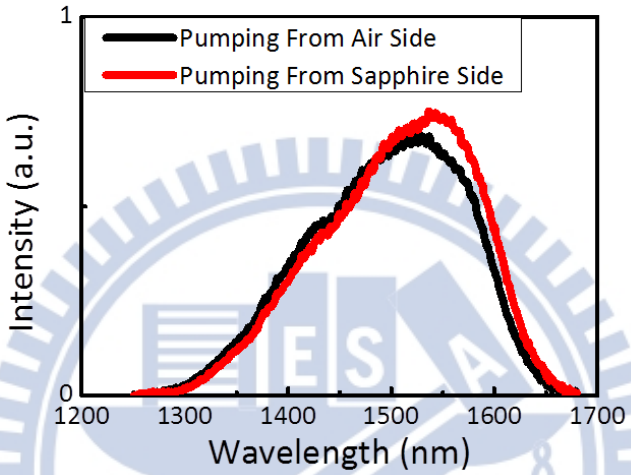

Figure 3-2 2 The PL pumped from air side is black line and pumped from sapphire side is red line.

The PL pumped from sapphire is higher about 10 pW than pumped from InGaAsP. Because the sapphire index is 1.7 that is higher than air. If InGaAsP layer at air layers center, the optics leaks some to both sides of the air. But the below of air layer changes the sapphire layer, the light more leak than the air layer, so the optical intensity is high pumped from sapphire. Figure 3-2 3 shows the light leak distribution diagram. And the sapphire has high transmission in NIR is shown in Figure 3-2 4.

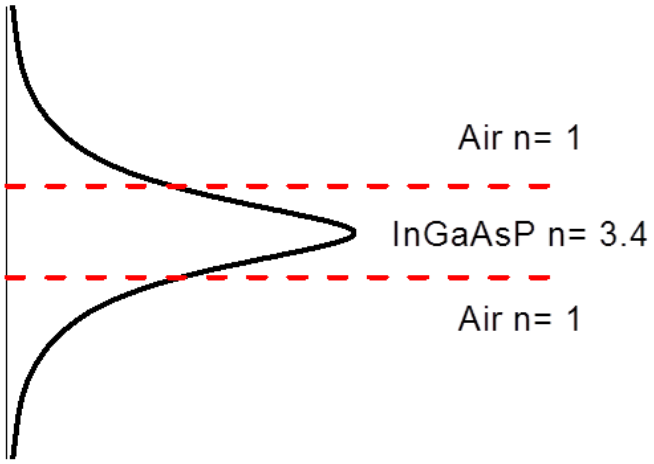

(a)

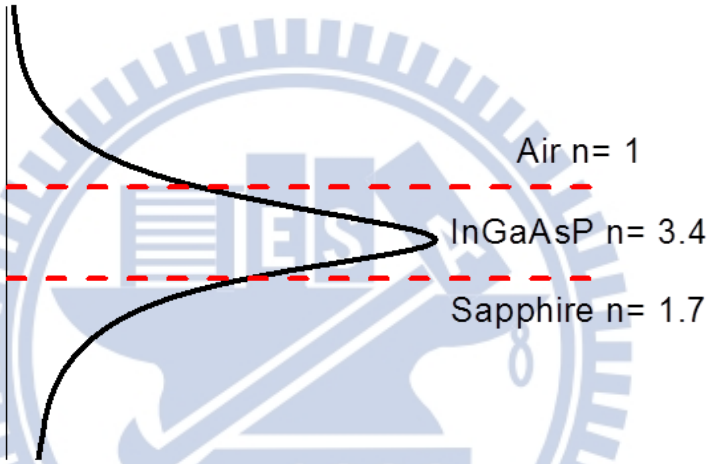

(b)

Figure 3-2 3 (a) Air-InGaAsP-Air and (b) Air-InGaAsP-Sapphire optical leak distributions.

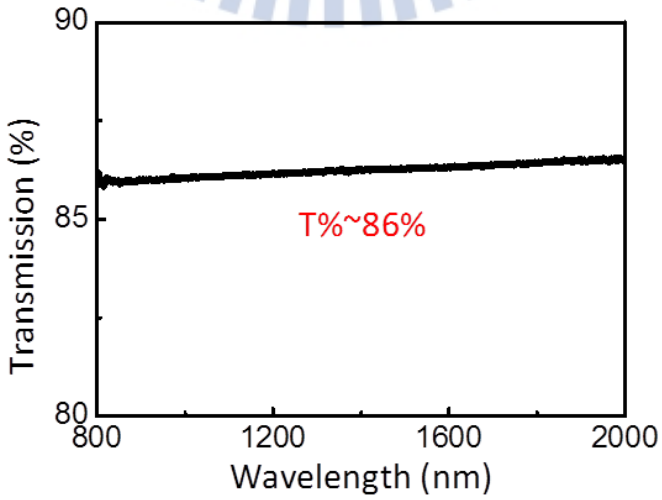

Figure 3-2 4 The sapphire the transmission spectrum in NIR

The leasing spectrum from the nano-ring cavity at room temperature is showed in the figure 3-2 5. The black line is pumped from air side, that lasing wavelength is about 1508.2 nm. And the red line is pumped from sapphire side, that lasing wavelength is about 1507.5 nm. The light in-light out curve (L-L curve) from the laser is shown in figure 3-2 6. The threshold power are 13 mW and 12.5 mW each of pumped from air and sapphire side. We confirm that lasing is worked with pumped from sapphire side.

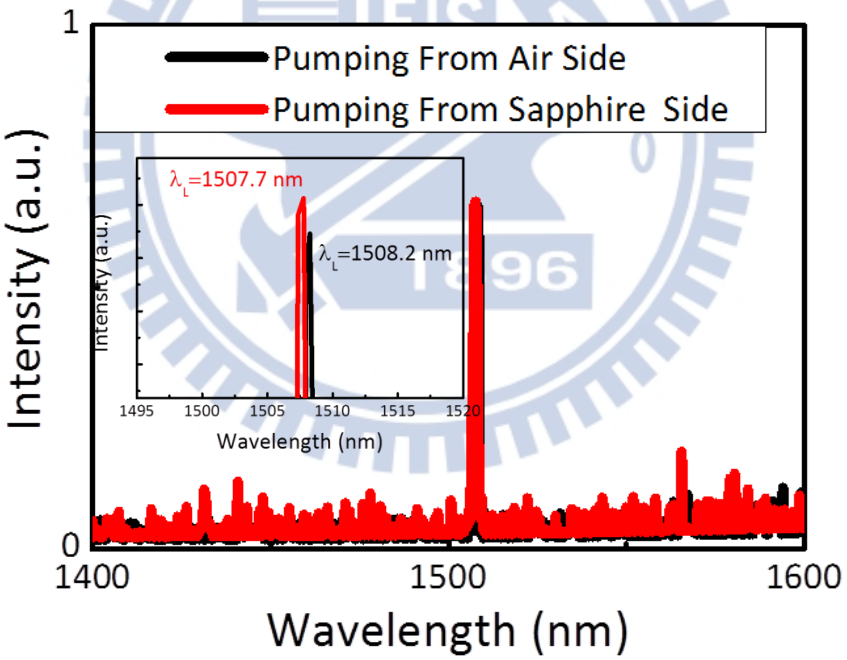

Figure 3-2 5 The black line is pumped from air side, that lasing wavelength is about 1508.2 nm. The red line is pumped from sapphire side, that lasing wavelength is about 1507.5 nm.

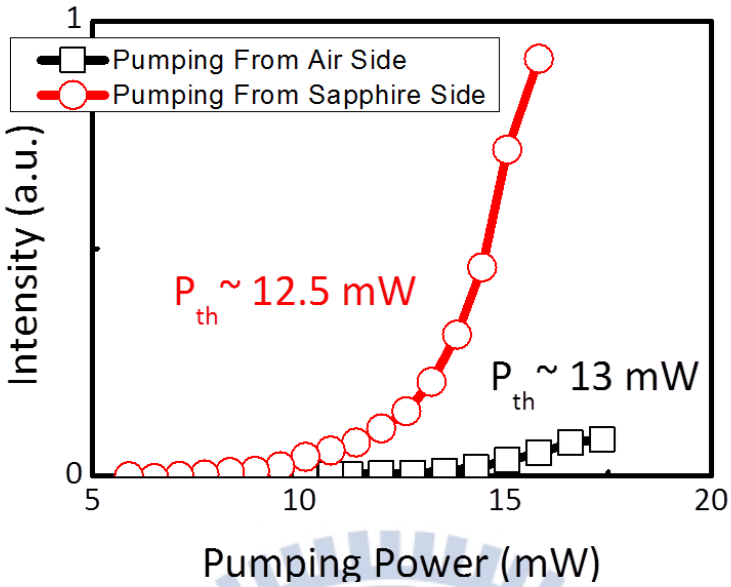

Figure 3-2 6 The threshold power are 13 mW and 12.5 mW each of pumped from air side and sapphire side.

3-3 Metal Nano-Ring Laser on Sapphire at 80K

Next, we coat the gold on nano-ring cavity is shown in figure 3-3 1, and the sample is putted in cryostate. It cans drop the temperature and control the temperature with liquid nitrogen in cryostate. The Figure 3-3 2 shows the sample putted in the cryostate.

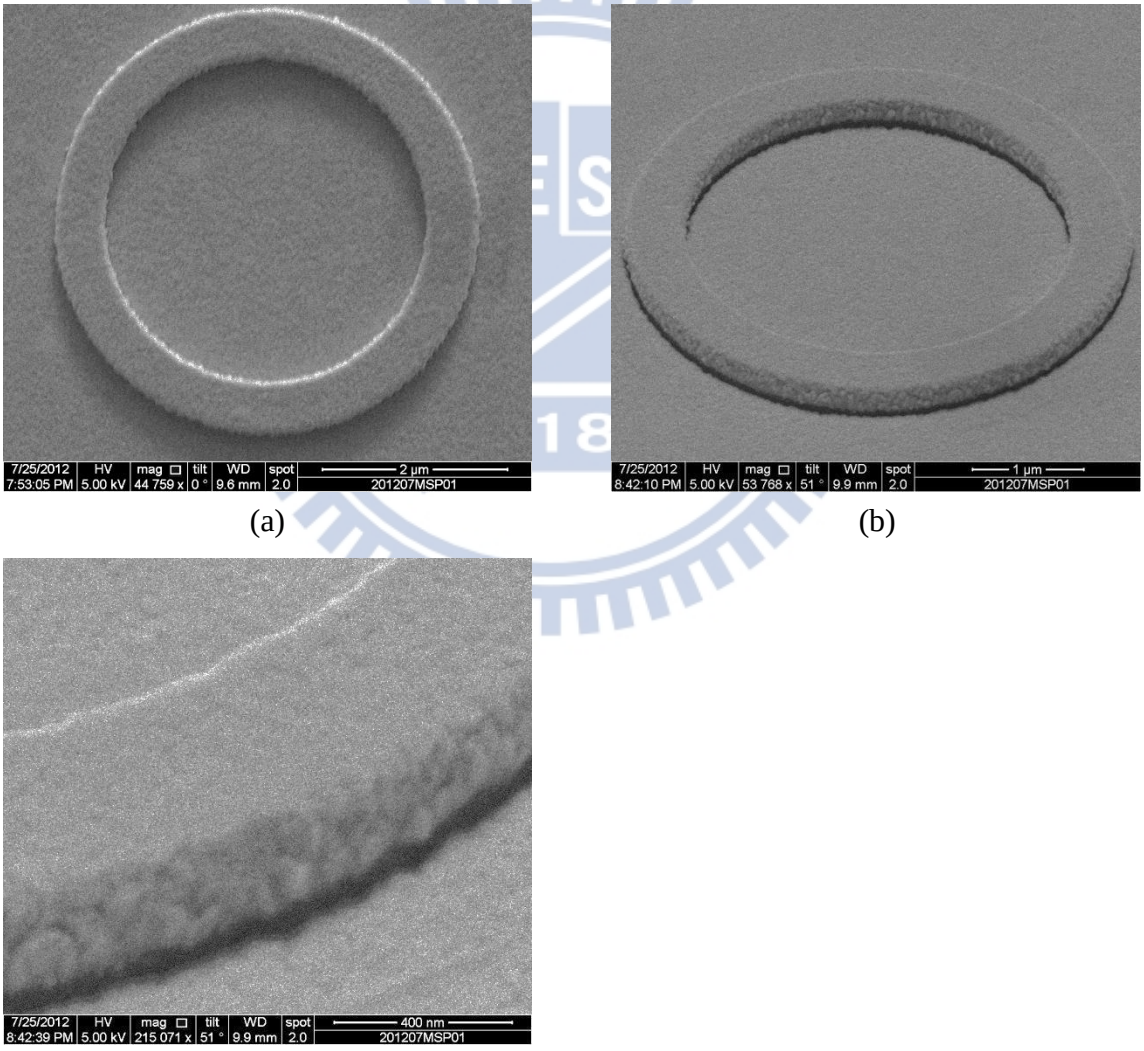

Figure 3-3. 1 SEM image of the coated gold nano-ring cavity. The thickness of gold is about 200 nm. (a) Top view and (b) (c) angle view of the nano-ring cavity.

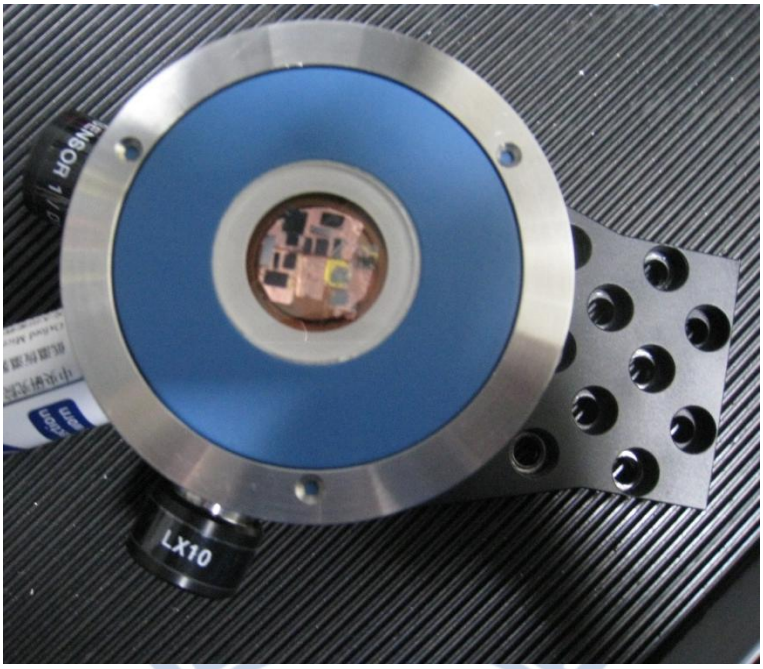

Figure 3-3 2 The sample is putted in the crystate.

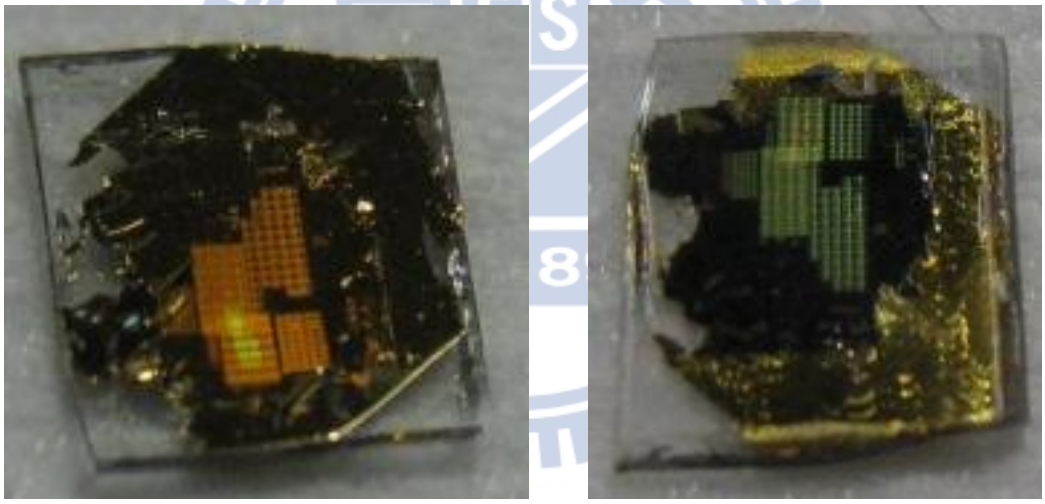

(a) (b)

Figure 3-3 3 The sample is after coating gold. Viewing of (a) is from gold and (b) is from sapphire.

The PL are pumped non coating from sapphire, pumped from gold, and pumped gold-coating from sapphire with the same input power at 80K that is shown in figure 3-3 4. The peak 1 PL at 1450nm is the InGaAsP quantum walls, and the peak 2 at 1250nm is the InGaAsP bulk. The PL of gold-coating is higher than non-coating because the gold is a very well reflection mirror in NIR, which can addition intensity from sapphire. Figure 3-3 5 shows reflection of Gold in NIR [32]. And the PL is pumped effect not well from gold side, but the PL intensity is outstanding in output efficiency from sapphire side. Because of the gold has low transmission in NIR that figure 3-3 6 shows gold transmission. Then we confirm the advantage of using the double polishing sapphire.

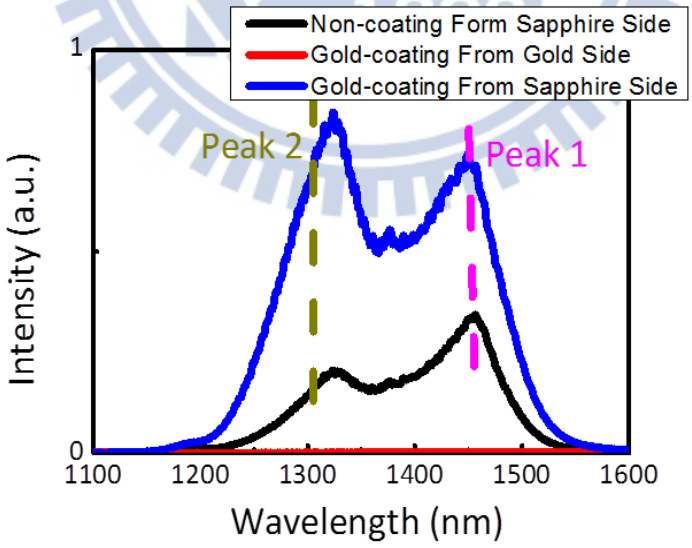

Figure 3-3 4 The PL pumped without gold from sapphire is black line, pumped from gold is red line, and pumped from sapphire is blue line.

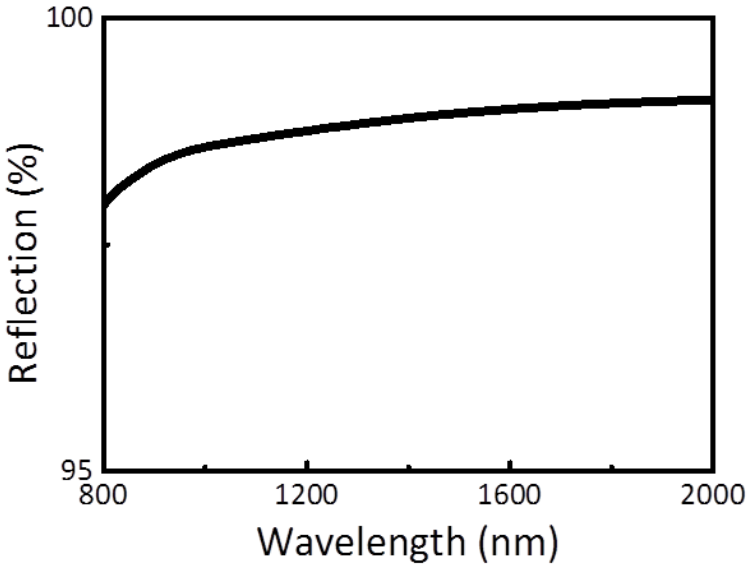

Figure 3-3 5 Reflection of gold in NIR

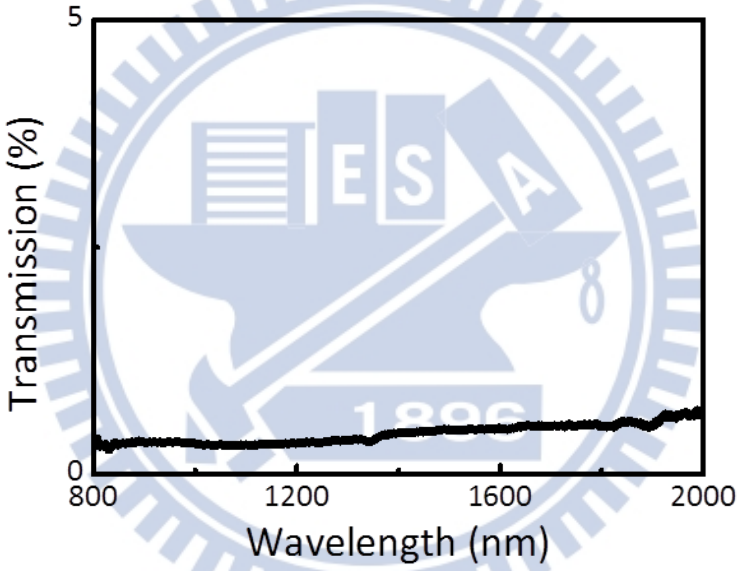

Figure 3-3 6 Transmission of gold in NIR

The pumped condition of each other is 6% duty cycle and 500 ns period at 80K. Because the sapphire-bonded device has better thermal conductivity, it can use high intensive intensity to pump, even use continuous wave. The figure 3-3 7 shows the lasing spectrums and L-L curve for the ring gold-coating and non-coating. The lasing wavelength is 1475.2 nm and threshold power is 1.3 mW for non-coating ring. The other is 1311 nm and threshold power is 8 mW.

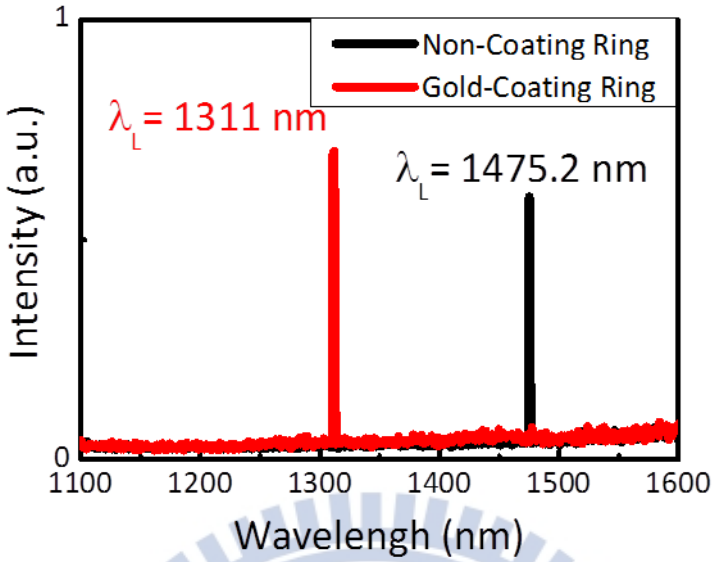

(a)

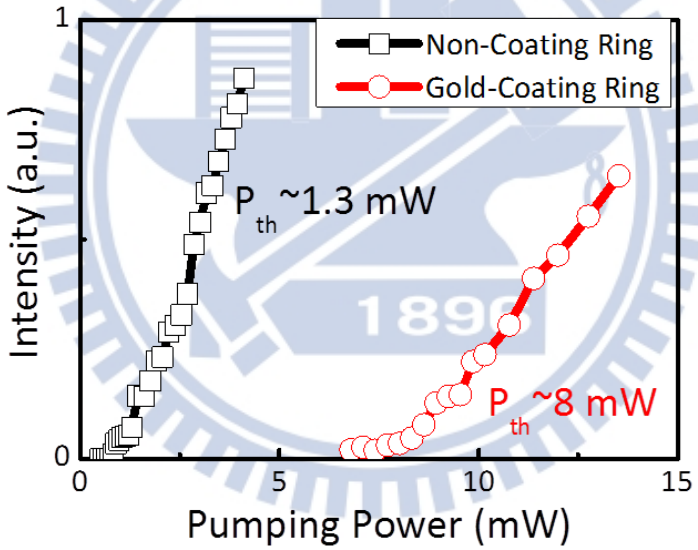

(b)

Figure 3-3 7 (a) The lasing wavelength are 1475.2 nm for non-coating ring, and 1311 nm for ring gold-coating ring. (b) The threshold power are 1.3 mW for non-coating, and 8 mW for ring gold-coating.

3-4 Simulation

We simulate the ring gold-coating and non-coating to confine the lasing mode is like mode profile use the finite element method (FEM). We simulate the mode profile with 3-D. Figure 3-4 1 (a) is illustrations of the non-coating ring on sapphire substrate, the diameter and width are 4 μm and 420 nm. Thickness of InGaAsP layer is 240nm and sapphire substrate thickness is 1μm. We use a quadrant of ring to instead of full ring, which can save memory and time. On the other hand, figure 3-4 1 (b) is illustrations of the non-coating ring on sapphire substrate, the diameter and width are 4 μm and 420 nm. Thickness of InGaAsP layer is 240nm, sapphire substrate thickness is 1 μm, and the gold thickness is 200 nm.

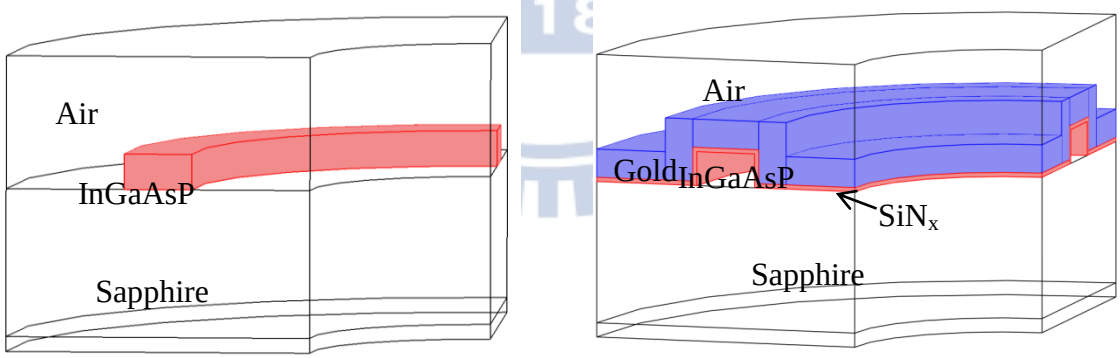

(a) (b)

Figure 3-4. 1 The simulation diagram. (a) is non-coating ring on sapphire and (b) is gold-coating ring on sapphire.

The simulation result of the non-coating ring is shown in figure 3-4 2, which is Whispering-Gallery (WG) mode. The lasing wavelength of measurement compare to the wavelength of simulation is shown in figure 3-4 3, the small difference between the experimental and simulation results. Because of it is not perfect in the fabrication, it has some roughness in the fabrication process, but it is smooth when simulation. And the simulation is not think about thermal. In fact, when we pumped the ring, and provide thermal at the same time.

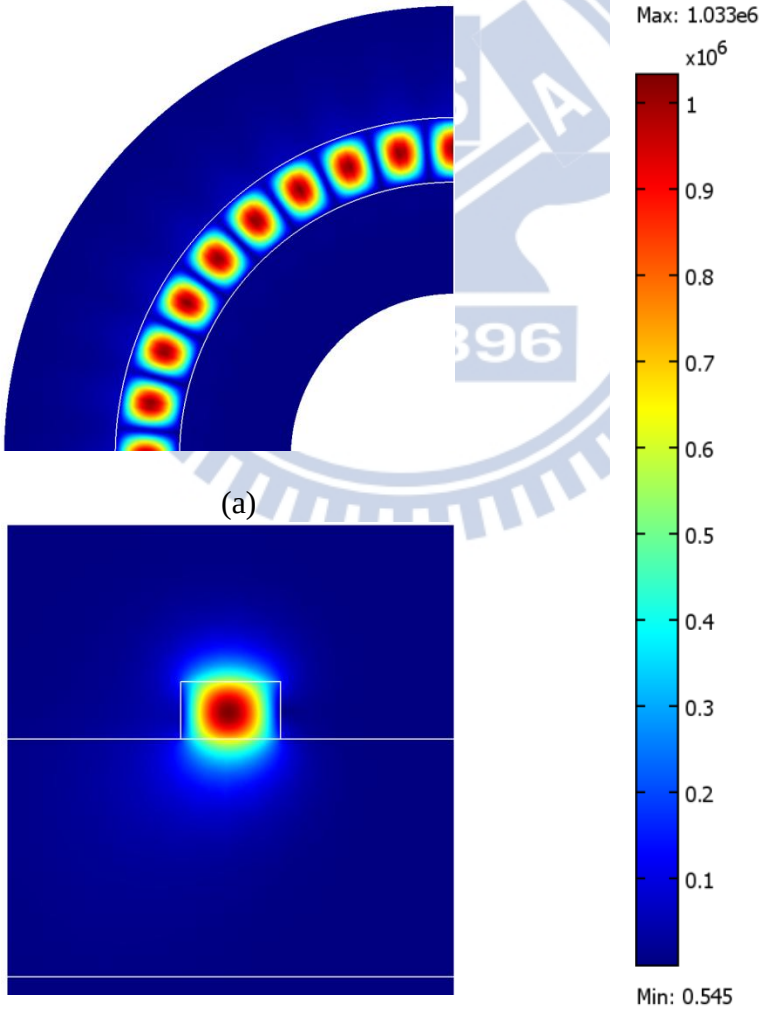

(a)

(b)

Figure 3-4 2 The normalize H field of the non-coating ring. (a) top view (b) side view.

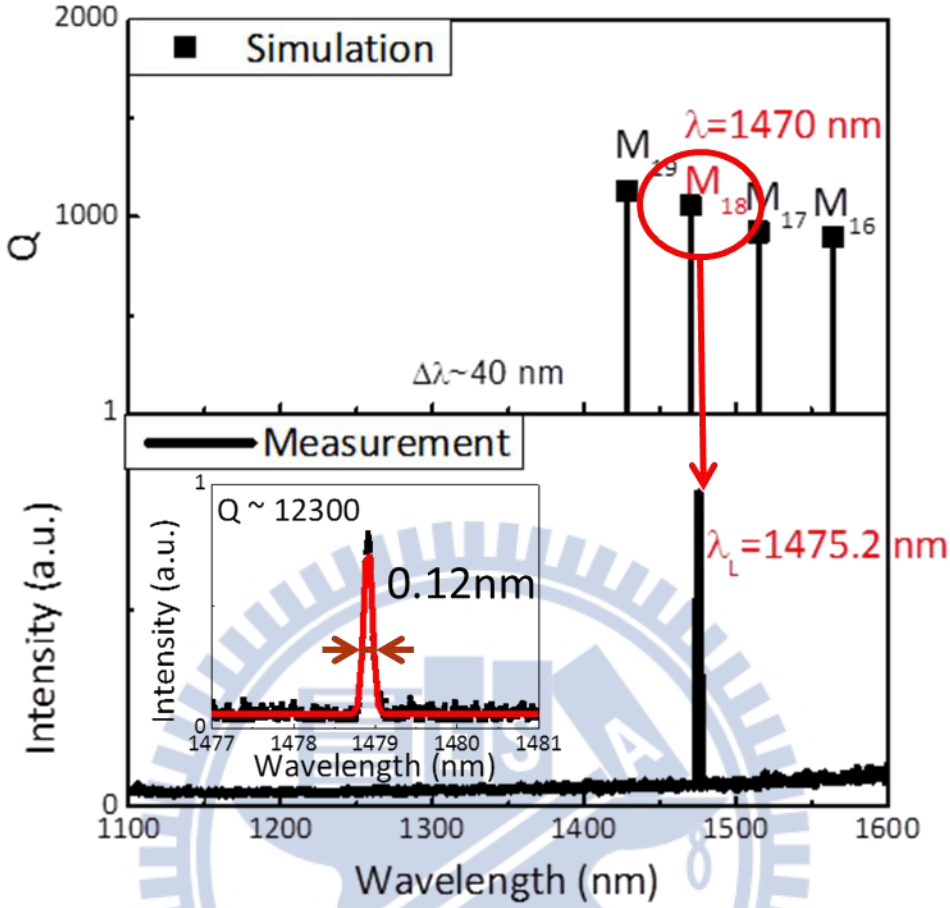

Figure 3-4 3 The measurement compares with simulation result. The lasing wavelength is 1478.9 nm and quality factor about 12300 for measurement. The wavelength is 1470 nm and quality factor about 1000 for simulation.

On the other hand, figure 3-4 4 shows the simulation result of the gold-coating ring. The mode profile shows normalize H field, which is WG mode at the same. The measurement result compares with the simulation is shown in figure 3-4 5, which are have error the same.

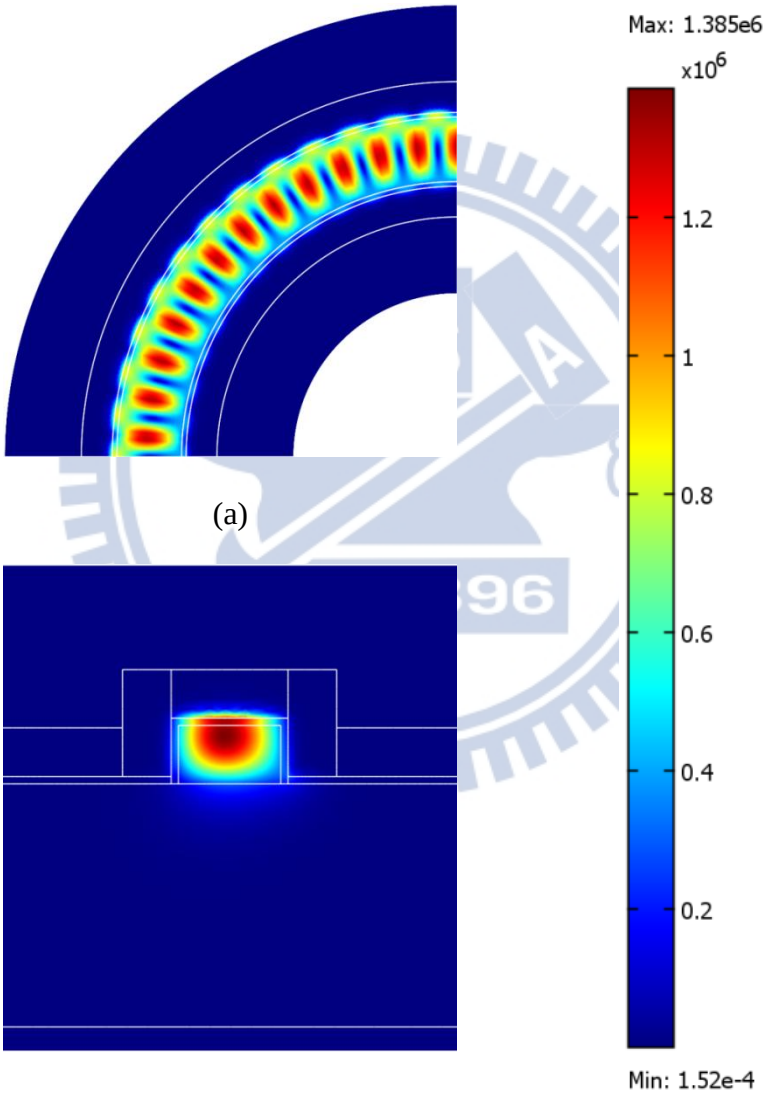

(a)

(b)

Figure 3-4 4 The normalize of H field. (a) top view (b) side view.

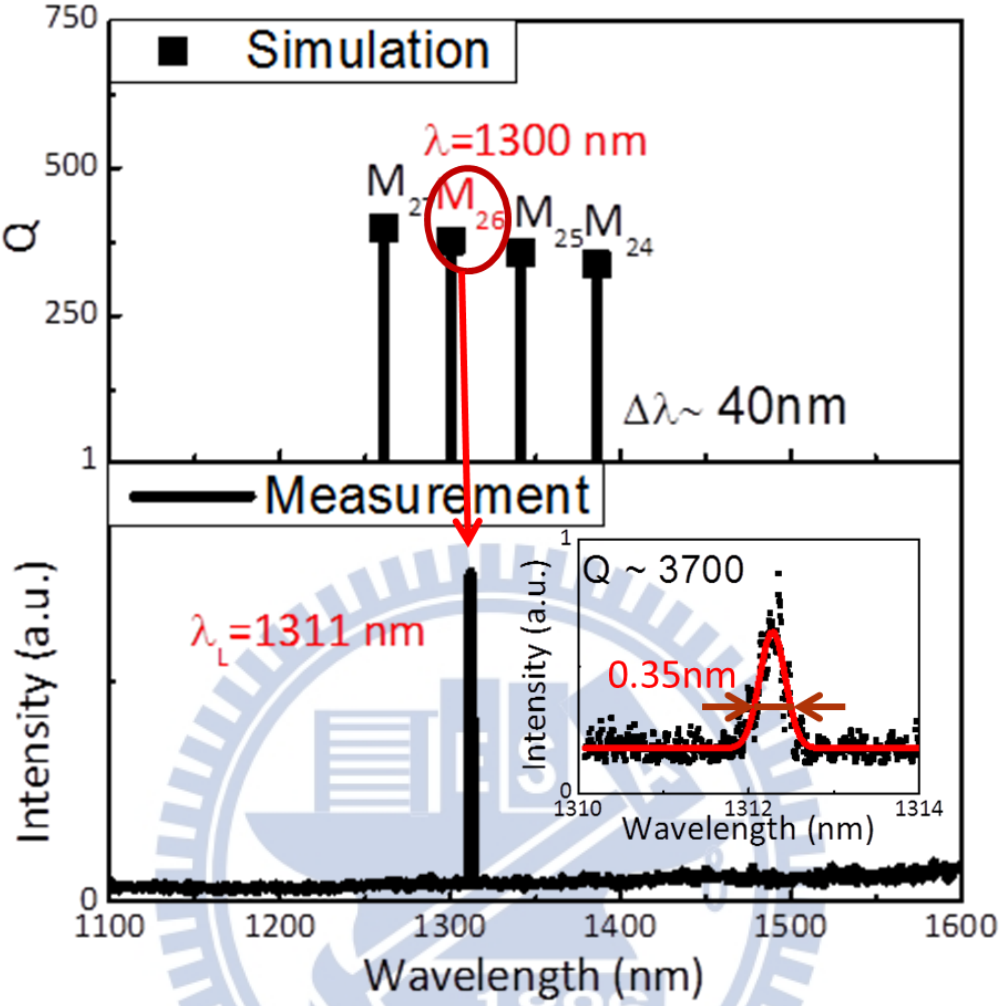

Figure 3-4 5 The measurement compares with simulation result. The lasing wavelength is 1311 nm and quality factor about 3700 for measurement. The wavelength is 1300 nm and quality factor about 400 for simulation.

The gold-coating ring compare with non-coating ring from side view with simulation. The figure 3-4 6 and the figure 3-4 7 show the direction of Z versus the intensity from side view. The intensity is strongest in center of MQWs/InGaAsP for the non-coating ring. but the gold-coating ring is not. The intensity is strongest at InGaAsP and gold interface, so we think that is hybird plasmon mode, it is not only at interface but aslo at InGaAsP. And simulation shows the intensity not leak to gold layer. Because of the gold absorption is high in NIR. The energy is not easy transmission.

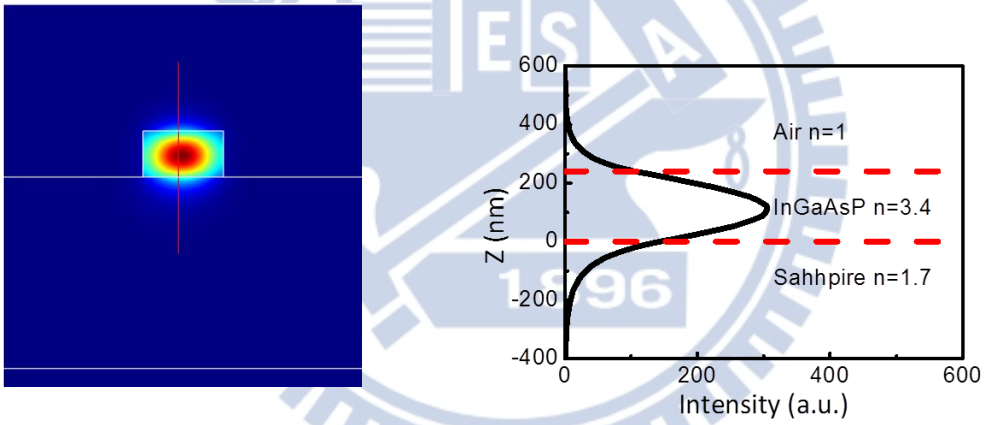

(a) (b)

Figure 3-4 6 (a) The mode profile of total energy. (b) The distribution of energy.

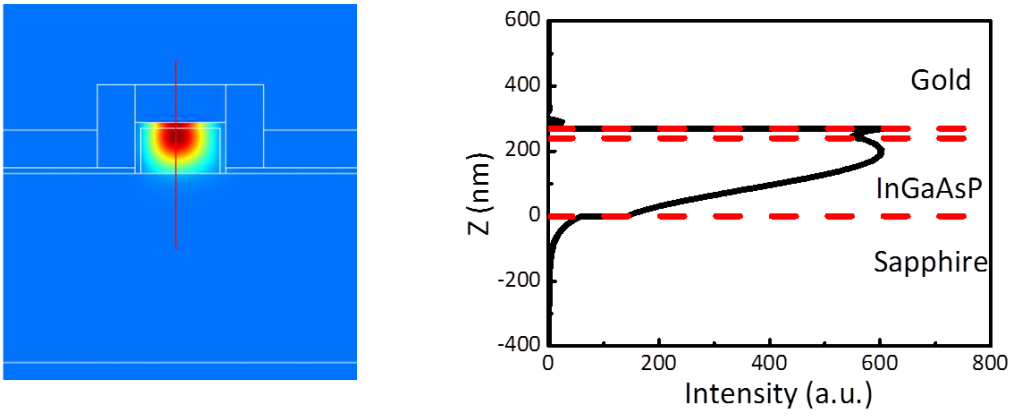

(a) (b

Figure 3-4 7 (a) The mode profile of total energy. (b) The distribution of energy.

3-5 Conclusion

In the chapter, we make a metal ring laser on sapphire at 80K. The sapphire has low index and high transmission in NIR. And it has higher pumped effect from sapphire side then from gold side. The lasing wavelength is 1311 nm and threshold power is 8 mW. We use FEM which can easy show approximately the mode profile for the gold-coating ring. The intensity is not only at InGaAsP but also at InGaAsP and gold interface, which shows side view of total energy. Next the chapter will discuss that the metal ring laser of thermal properties.

Chapter 4 Thermal Properties of Gold-Coating Ring on Sapphire

In the chapter, we will discuss the thermal property for gold-coating ring and only ring on sapphire. The lasing wavelength is shifted with temperature and pumping power variation individually. Then we use the $\Delta T/\Delta P$ (K/mW) to estimate the thermal resistance. And we compare the measurement with the simulation result.

4-1 Temperature-Dependent Lasing Wavelength

Last the chapter we make a metal ring on sapphire at 80K. Next, we will change temperature that lasing wavelength shifting with temperature variation. At first, figure 4-1 1 shows the PL with temperature. The wavelength is red shift with temperature. The $\Delta\lambda/\Delta T$of peak 1 is 0.46 nm/K for non-coating of PL, and 0.48 nm/K for gold-coating of PL is shown in the figure 4-1 2 (a).And The $\Delta\lambda/\Delta T$of peak 2 is 0.57 nm/K for non-coating of PL, and 0.53 nm/K for gold-coating of PL is shown in the figure 4-1 2 (b)

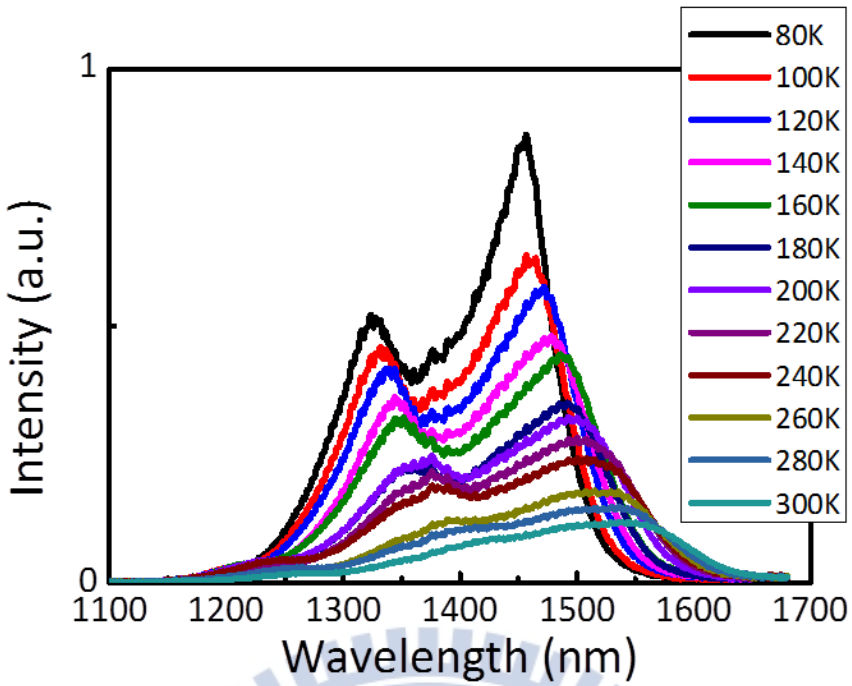

(a)

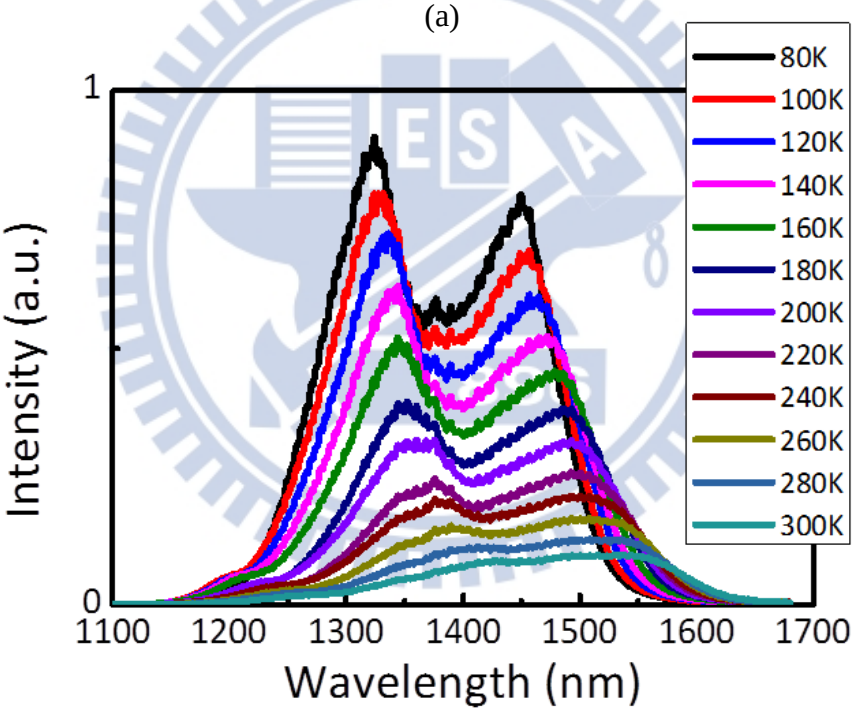

(b)

Figure 4-1 1 The PL wavelength shifts with temperature variation of the ring (a) non-coating and (b) gold-coating.

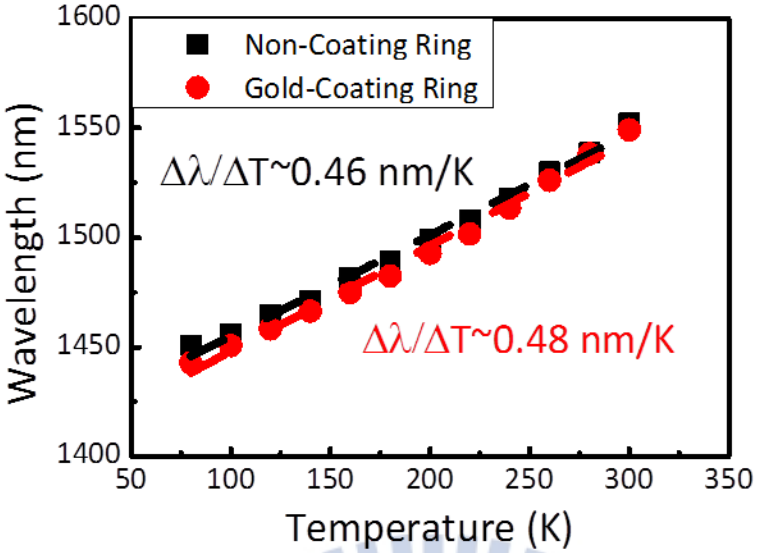

(a)

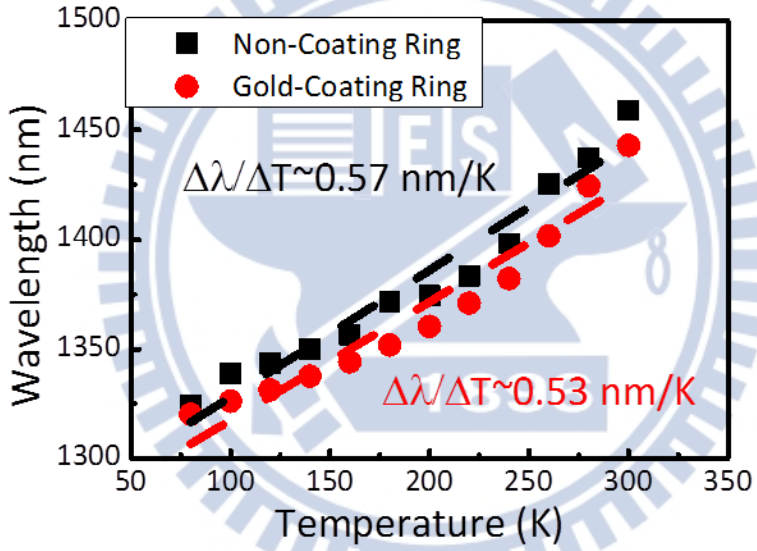

(b)

Figure 4-1 2 The PL wavelength shifts with temperature variation of the non-coating is black point and gold-coating is red point. (a) is peak 1 that the $\Delta\lambda/\Delta T$ are 0.46 nm/K non-coating and 0.48 nm/K gold-coating. (b) is peak 2 that the $\Delta\lambda/\Delta T$ are 0.57 nm/K non-coating and 0.53 nm/K gold-coating.

The wavelength shifts with temperature variation for the non-coating ring on sapphire, which is shown in figure 4-1 3. The $\Delta\lambda/\Delta T$ is 0.063 (nm/K). The non-coating ring is lasing at room temperature, which does not have metal loss, and the quantum walls of InGaAsP have supply gain. So the non-coating ring on sapphire can work from 80K to room temperature.

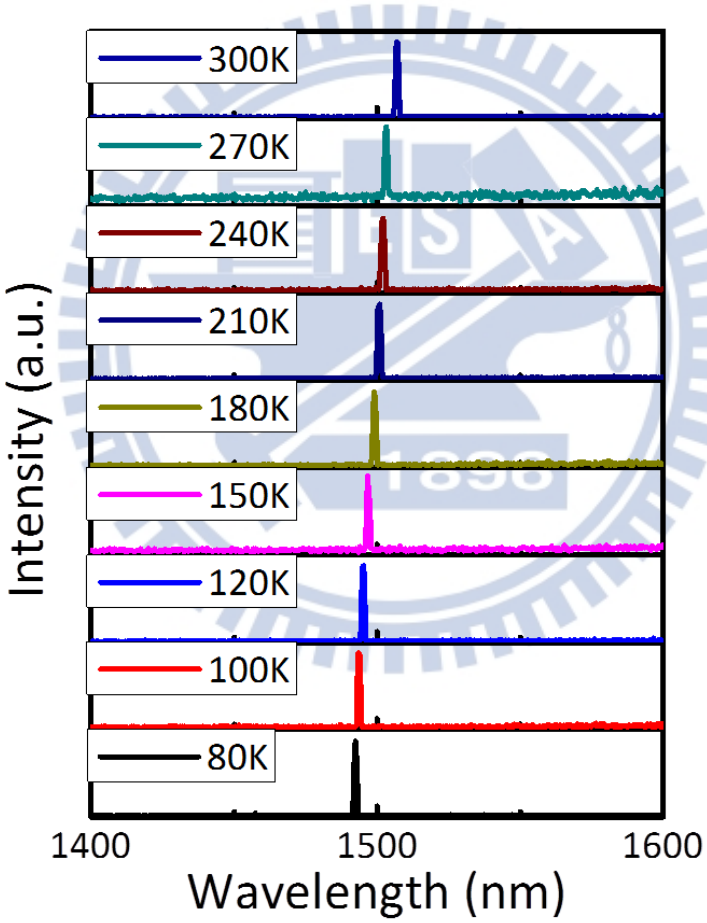

Figure 4-1 3 The lasing wavelength shifts with the temperature variation for non-coating ring. The temperature changes from 80K to 300K. The lasing wavelength is from 1492 nm to 1507 nm.

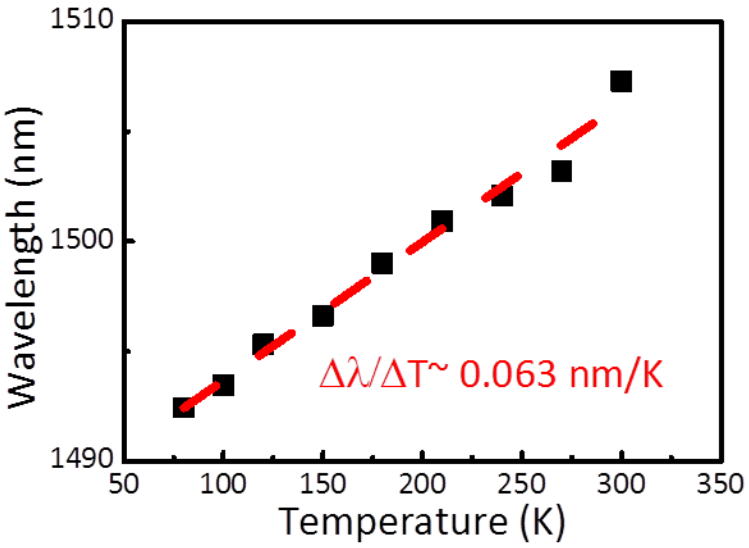

Figure 4-1 4 The lasing wavelength shifts with temperature variation. The temperature changes from 80K to 300K, and $\Delta\lambda/\Delta T$ is 0.063 nm/K.

And figure 4-1 5 shows the wavelength with temperature is 0.026 (nm/K) for the gold-coating ring on sapphire. But the metal ring laser is not working at temperature above 140K that we have pumping power now. The lasing wavelength is from 1311 nm to 1313 nm. The metal loss is high in NIR and quantum walls of InGaAsP lass are too high to work. So it doesn't work at high temperature.

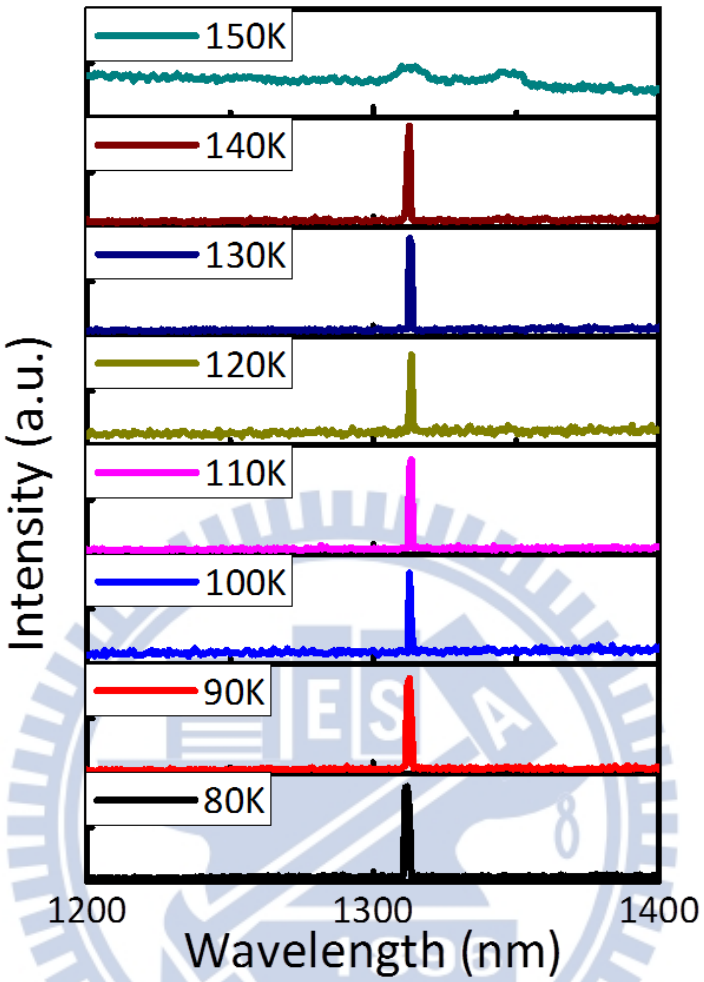

Figure 4-1 5 The lasing wavelength shifts with temperature variation. The temperature changes from 80K to 150K. The lasing wavelength is from 1311 nm to 1313 nm.

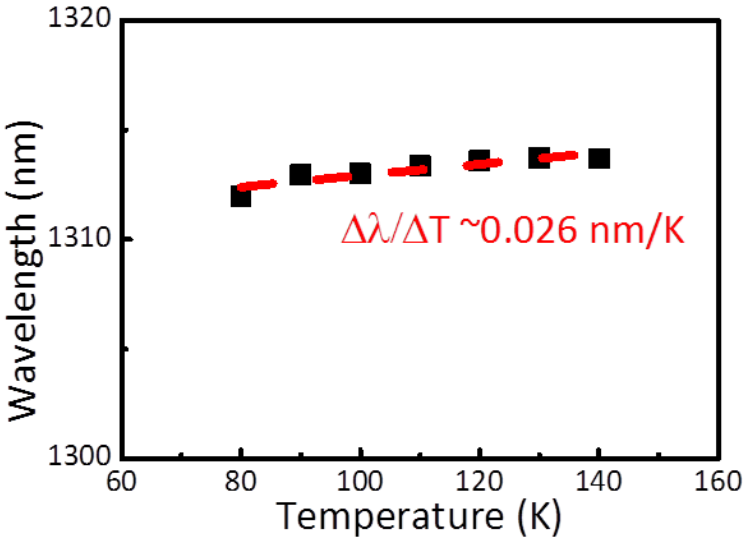

Figure 4-1 6 The lasing wavelength shifts with temperature variation. The temperature changes from 80K to 140K, and $\Delta\lambda/\Delta T$ is 0.026 nm/K.

The slope is slowed than the non-coating ring. It has two parameters that one is absorption with temperature. The other one is material thermal property. In order to the trend is true. We simulate the wavelength with temperature use FEM. In the simulation, we consider the material absorption with temperature, which InGaAsP absorption coefficient is $n = 3.202 + 7 \times 10^{-5}T + 2 \times 10^{-7}T^2$ [33], and gold absorption coefficient is $n = \sqrt{((Au\ real)^2 - (Au\ imag)^2) - 2RTi(Au\ real)(Au\ imag)/2.271}$ [14]. The wavelength with temperature is shown in figure 4-1 7. Figure 4-1 7 (a) is measurement compares with simulation of the non-coating ring, and (b) is the gold-coating ring. The simulation trend is the same compared with our measurement. The measurement and simulation result have some error that only thinks about absorption with temperature, not consider thermal property in simulation.

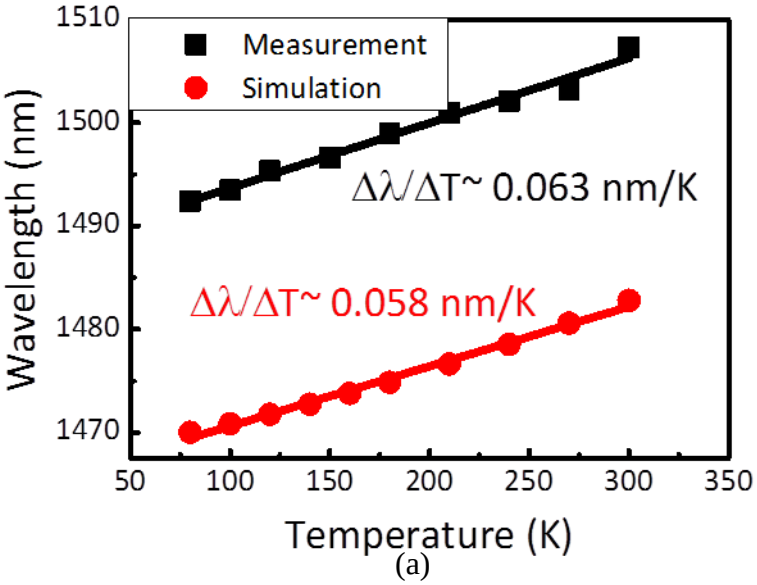

(a)

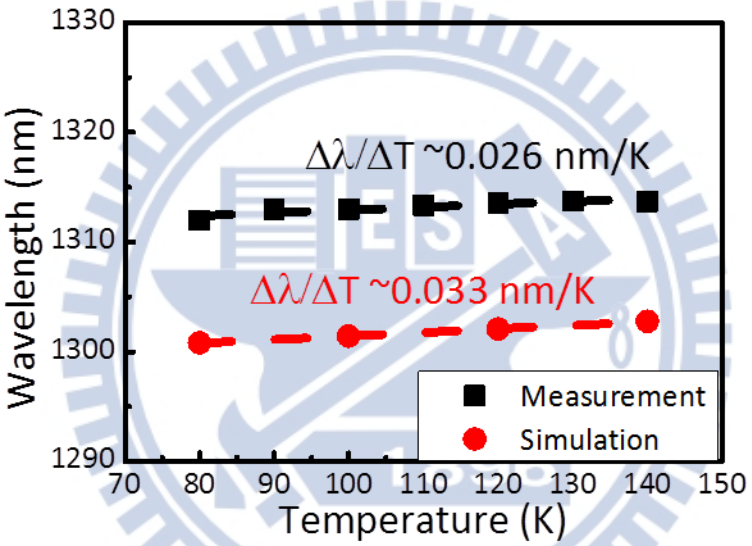

(b)

Figure 4-1 7 The lasing wavelength shifts with temperature variation. The measurement compares with simulation of the ring (a) non-coating and (b) gold-coating.

4-2 Pumping Power-Dependent Lasing Wavelength

The next, we will change pumping power to observe laser wavelength shifting at the some temperature. The pumped condition is duty 6% and 500ns period at 80K. At the first, figure 4-2 1 (a) shows the lasing wavelength shifts with pumping power variation of the non-coating ring that $\Delta\lambda/\Delta P$ is 0.151 (nm/mW).

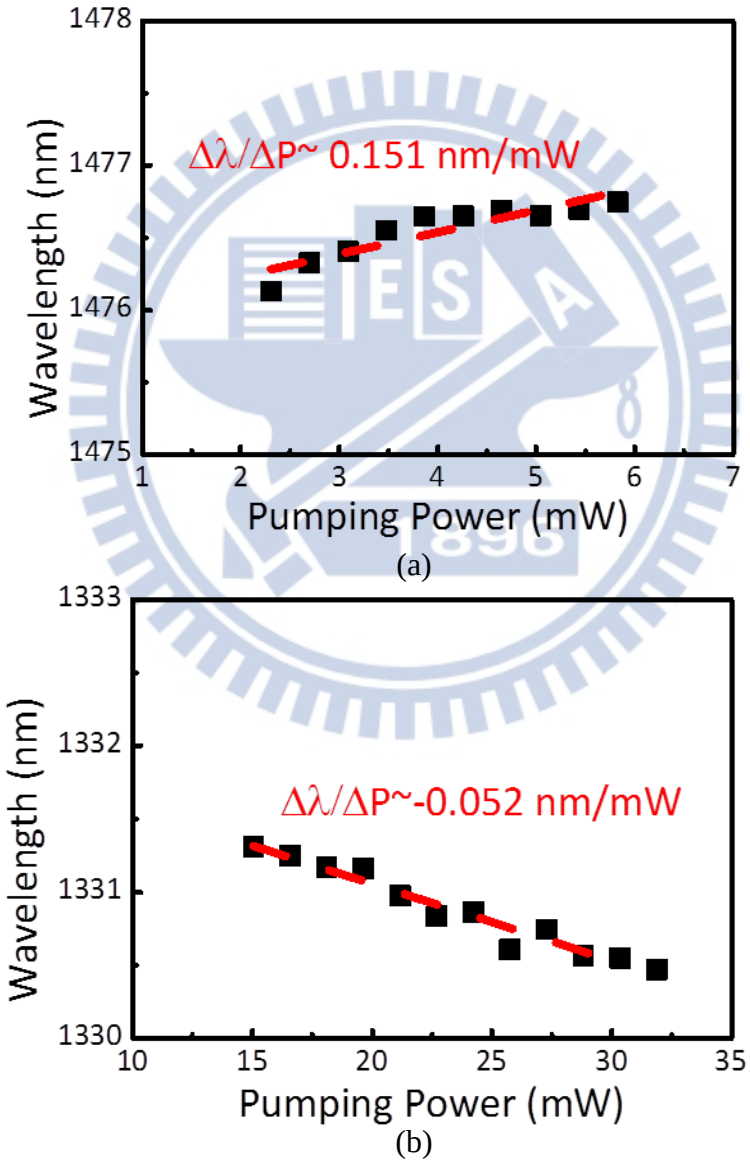

Figure 4-2 1 The lasing wavelength shifts with pumping power variation. (a) The $\Delta\lambda/\Delta P$ is 0.151 (nm/mW) of the non-coating ring. (b) The $\Delta\lambda/\Delta P$ is -0.052 (nm/mW) of gold-coating ring.

And figure 4-2 1 (b) shows the lasing wavelength shifts with pumping power variation of the gold-coating ring that $\Delta\lambda/\Delta P$ is -0.052 (nm/mW). The non-coating ring has a red shift as the pumping power increase, but the gold-coating ring has a blue shift as the pumping power increase that is not explain now. But the slope of $\Delta\lambda/\Delta P$ is flatter for gold-coating ring than the non-coating ring is true. It has higher thermal conductivity than the non-coating ring on sapphire.

The gold layer has high thermal conductivity than sapphire, so the heat cans easy conduct quickly by gold layer at high pumping power. But the ring without Au that heat only conducts by sapphire layer. We use simulation to confirm our opinion. The parameters show in table 4-2 1. Figure 4-2 2 shows illustrations of the non-coating ring on sapphire, and figure 4-2 3 shows gold-coating.

Material	Thermal Conductivity (W/m-K)	Density (Kg/m^3)	Heat Capacity (J/Kg-K)
Air	0.0262	1.1758	1015.415
InGaAsP	4.2	5088.4	334.8
Sapphire	50	3965	730
SiN_x	30	3100	710.6
Gold	332	19300	129

Table 4-2 1 The simulation parameters.

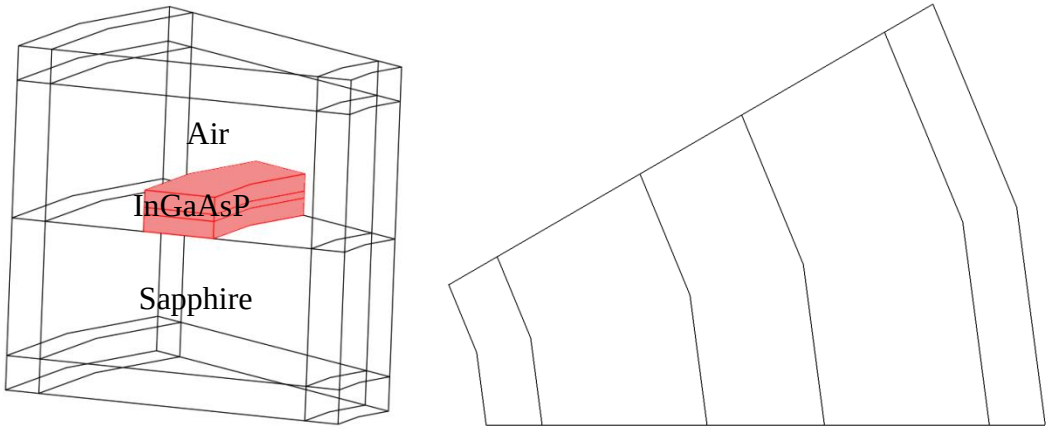

Figure 4-2 2 The non-coating ring on sapphire (a) 3-D view (b) top view.

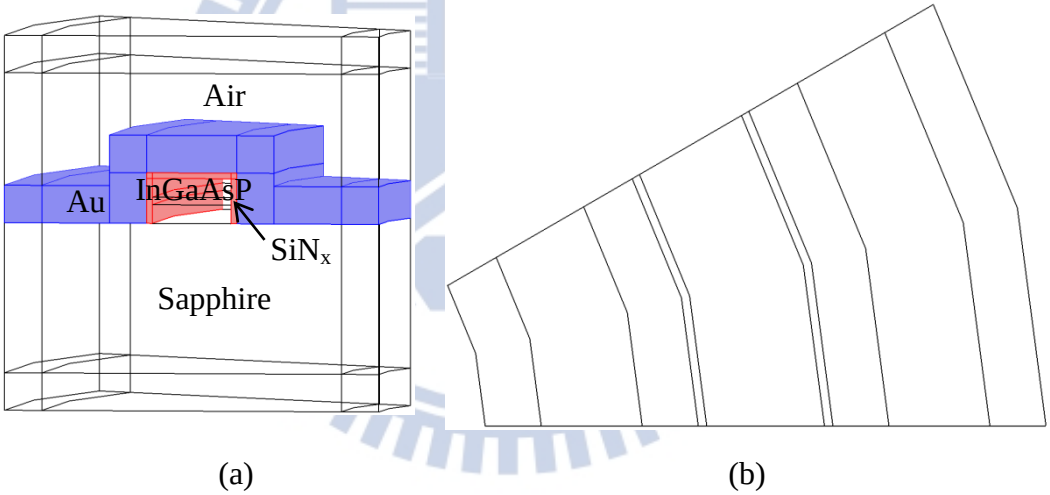

Figure 4-2 3 The gold-coating ring on sapphire (a) 3-D view (b) top

The simulation result is shown figure4-2 4 (a) (b) the non-coating ring. The arrows represent heat fluxes, which the major part of heat fluxes through sapphire layer. The highest temperature is 380K. If compare with the gold-coating ring that the highest temperature is 333K, which is lower than non-coating ring. The heat fluxes of gold-coating ring main through gold layer, secondary through sapphire layer is shown in figure 4-2 4 (c) (d). At the same color bar, the non-coating ring is hotter than gold-coating ring.

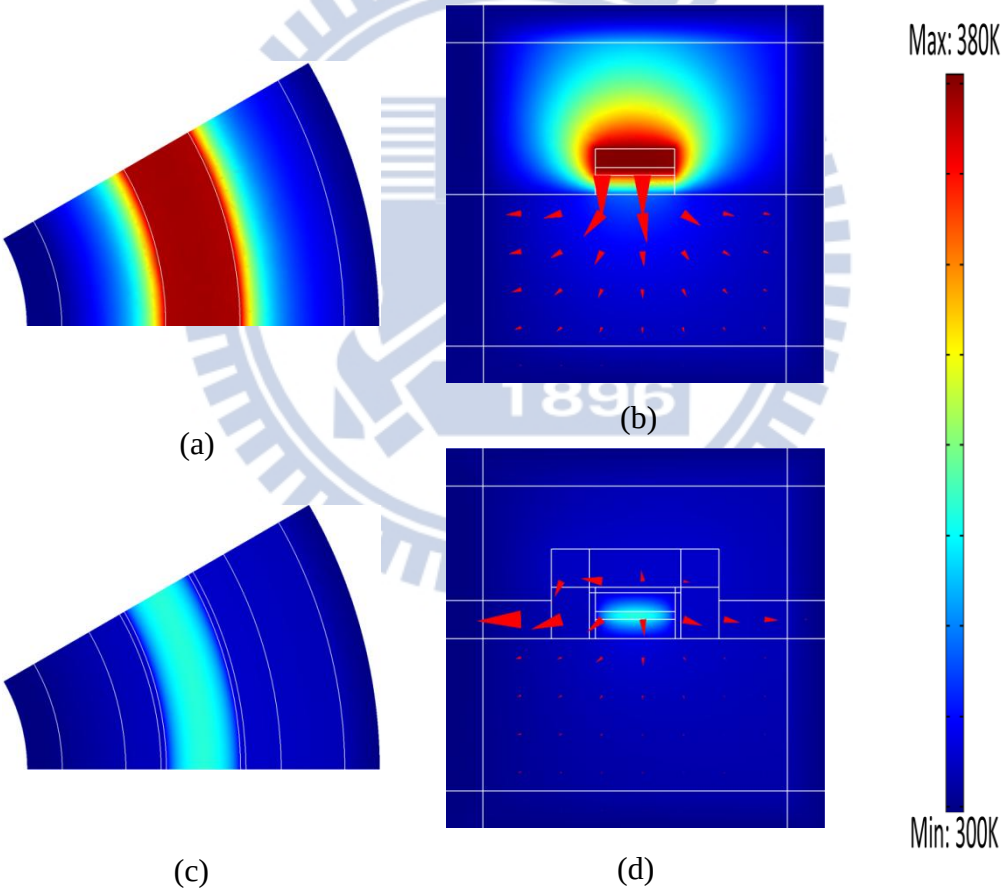

Figure 4-2 4 The heat fluxes distribution for non-coating ring on sapphire (a) top view and (b) side view. The highest temperature is 380K. The major of heat heats are through sapphire layer. And the heat fluxes distribution for gold-coating ring on sapphire (c) top view and (d) side view. The highest temperature is 330K. The major of heat heats are through gold layer, secondary through sapphire layer.

4-3 Thermal resistance of Gold-Coating Ring

With above conclusion, definition of thermal resistance is $R = \Delta T/\Delta P$ (K/mW), means temperature change with per unit power. So we can redefinition of thermal resistance is $\frac{\Delta T}{\Delta P} = \frac{\Delta T}{\Delta \lambda} \times \frac{\Delta \lambda}{\Delta P}$ [34], where λ is lasing wavelength. Then, we can use to control temperature to observe lasing wavelength shifting, which obtains $\Delta\lambda/\Delta T$ (nm/K). And we can control pumping power at the same temperature to observe lasing wavelength shifting, which obtains $\Delta\lambda/\Delta P$ (nm/mW). The two terms are easy use measurement to obtain.

The chapter 4-1, lasing wavelength shifts with temperature variation, and the chapter 4-2, which lasing wavelength shifts with pumping power variation. We use the results to estimate thermal resistance for the ring non-coating and gold-coating. Figure 4-3 1 shows the lasing wavelength shifts with temperature variation, which the $\Delta\lambda/\Delta T$ is about 0.063 (nm/K). On the other hand, lasing wavelength shifts with pumping power variation, which the $\Delta\lambda/\Delta P$ is about 0.151 (nm/mW). The thermal resistance is 2.4 (K/mW) for the non-coating ring on sapphire. Figure 4-3 2 shows the lasing wavelength shifts with temperature variation, which the $\Delta\lambda/\Delta T$ is about 0.028 (nm/K). On the other hand, lasing wavelength shifts with pumping power variation, which the $\Delta\lambda/\Delta P$ is about -0.052 (nm/mW). The thermal resistance is 1.8 (K/mW) for the ring with Au on sapphire.

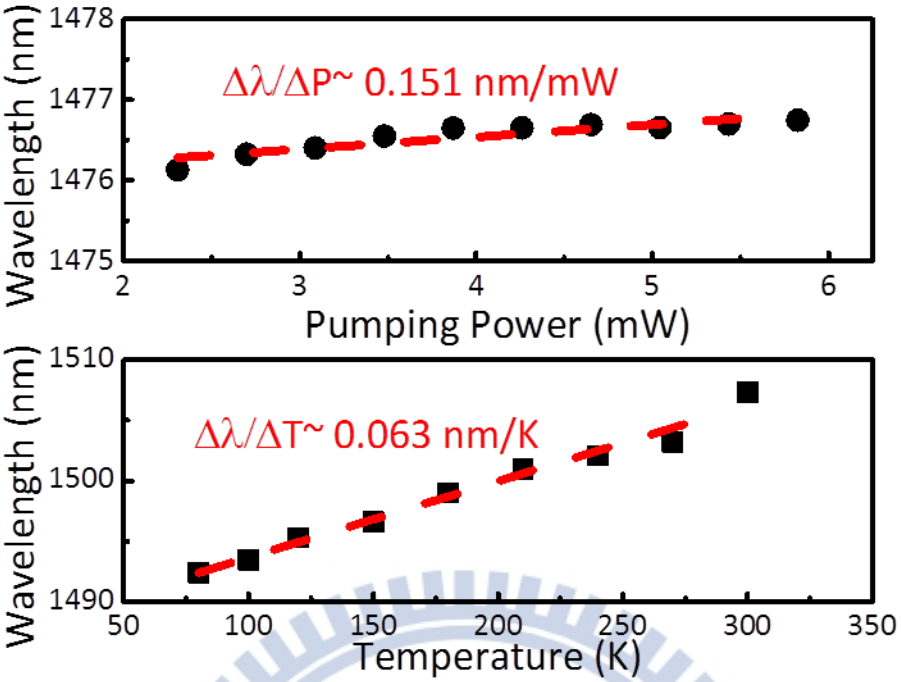

Figure 4-3 1 The non-coating ring on sapphire. The $\Delta\lambda/\Delta T$ is about 0.063 (nm/K), and the $\Delta\lambda/\Delta P$ is about 0.151 (nm/mW).

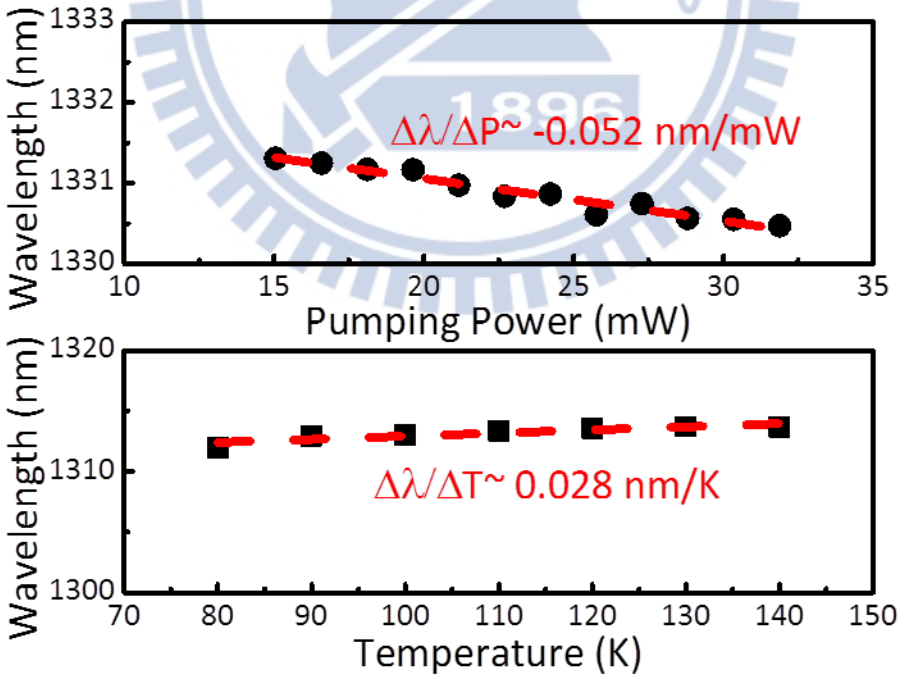

Figure 4-3 2 The gold-coating ring on sapphire. The slope $\Delta\lambda/\Delta T$ is about 0.028 (nm/K), and the slope $\Delta\lambda/\Delta P$ is about -0.052 (nm/mW).

The thermal resistance is lower for gold-coating ring than the non-coating ring. Although, the sapphire is a pretty good of thermal conductivity material, but the gold is better than the sapphire. So the main part of heat fluxes is through gold layer. Then we use the simulation that temperature by changing the pumping power to estimate $\Delta T/\Delta P$. Figure 4-3 3 shows $\Delta T/\Delta P$ that black points are 80 K/mW for non-coating ring , and red points are 33 K/mW for gold-coating ring. The simulation proves that has lower thermal resistance when addition Au layer at the same.

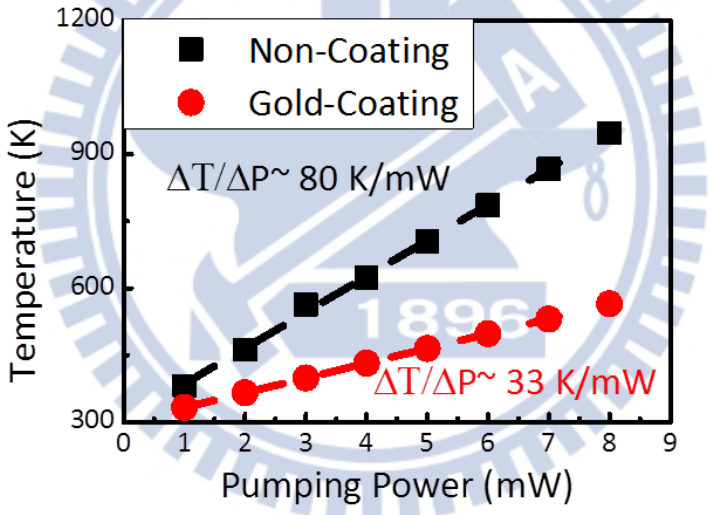

Figure 4-3 3 With simulation to estimate $\Delta T/\Delta P$ that black points are 80 K/mW for non-coating ring, and red points 33 K/mW for gold-coating ring.

Structure / Thermal resistance	Without Au	With Au
Measurement (Pulse)	2.4 (K/mW)	1.8 (K/mW)
Simulation (CW)	80 (K/mW)	33 (K/mW)

Table 4-3 1 The thermal resistance compares measurement with simulation.

4-4 Conclusion

In the chapter, we discuss thermal resistance use $\Delta T/\Delta P$ to obtain. Then will $\Delta T/\Delta P$ be divided $\Delta T/\Delta\lambda$ and $\Delta\lambda/\Delta P$. The two terms are easy obtaining that use measurement. The first, the lasing wavelength shifts with temperature variation in crystate. The $\Delta\lambda/\Delta T$ are 0.063 (nm/K) for non-coating ring on sapphire and 0.028 (nm/K) for gold-coating ring on sapphire. Then, the lasing wavelength shifts with pumping power variation at the same temperature. The $\Delta\lambda/\Delta P$ are 0.151 (nm/mW) for non-coating ring on sapphire and -0.052 (nm/K) for gold-coating ring on sapphire. Final, it obtains thermal resistance($\Delta T/\Delta P$) that non-coating ring on sapphire is 2.4 (K/mW) and gold-coating ring on sapphire is 1.8 (K/mW). But we cannot explain why the $\Delta\lambda/\Delta P$ is blue shift now. We use simulation to observe the heat fluxes. The main part of heat fluxes is conduct by sapphire layer for non-coating ring, and gold-coating ring is main conduct by gold layer.

Chapter 5 Conclusion and Outlook

In this thesis, we has demonstrated a structure that gold-coating ring laser bonding on double polish sapphire, which has low index and high transmission in NIR. Comparing with reported metal lasers, this laser is outstanding in output efficiency from sapphire side. It through a series of the fabrication process including the wafer bonding, E-beam lithography, ICP-RIE dry etching, and thermal deposition. And the lasing characteristic is obtained by pumping from sapphire at 80K and discussed. With simulate to observe lasing mode profile.

In this metal laser, amount of heat flux dissipate through metal layer was predicted by 3D FEM simulation, but non-coating ring is by sapphire layer because air has a low thermal conductivity. And observed by comparing experimental results between lasers with and without coating laser.

According experimental results, thermal resistance was estimated by measuring lasing wavelength shifting with temperature and pumping power variation individually, the thermal resistance of the gold coating ring laser is 1.8K/mW.

In the future, let the intensity shift to gain medium in center that try to lasing turn on at room temperature and shrink the ring diameter. The $\Delta\lambda/\Delta P$ is blue shift phenomenon when change pumping power for gold-coating ring on sapphire that is the other of parts have to solve. Next, the metal-coating device has high thermal conductivity and low thermal resistance, which can try to make the electrically pumping device. The simulation should concern not only optical effect and also thermal effect at the same time. Let result can match the measurement result.

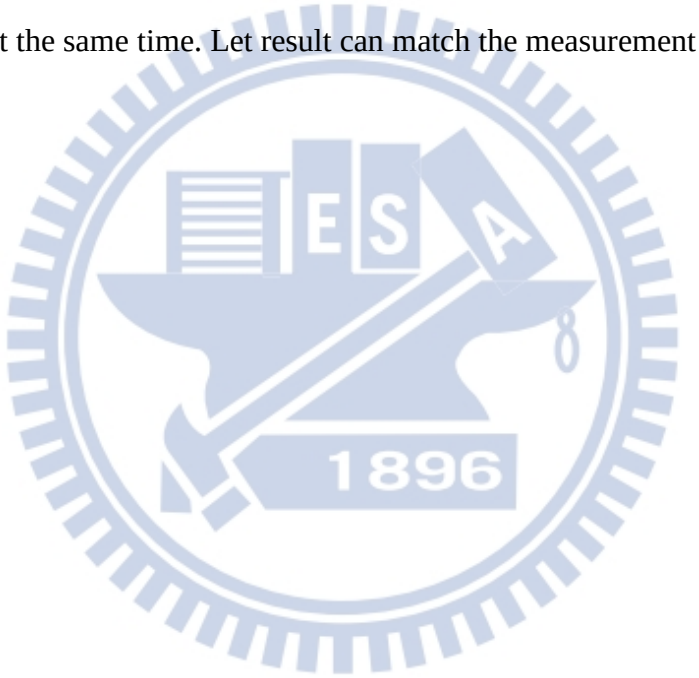

References

[1] http://technotechz.blogspot.tw/2011/01/6-common-storage-technologies.html

[2] http://ilasikym.blogspot.tw/2009/11/q.html

[3] http://www.laser.org.tw/laser/magazine/laser_application-vol6/vol6-017.htm

[4] http://www.sensorsinc.com/fsotracking.html

[5] K. Iga, "Surface-emitting laser—its birth and generation of new optoelectronics field," **IEEE Journal on Selected Topics in Quantum Electronics**, 6, 1201–1215 (2000)

[6] Masayuki Fujita, Atsushi Sakai, and Toshihiko Baba, "Ultrasmall and ultralow threshold GaInAsP–InP microdisk injection lasers: design, fabrication, lasing characteristics, and spontaneous emission factor," I**EEE J. Selected Topics in Quantum Electronics**, 5, 673-681 (1999)

[7] J. D. Joannopoulos, S. G. Johnson, J. N. Winn, and R. D. Meade, "Photonic crystals," Princeton University Press, (2008)

[8] O. Painter R. K. Lee A. Scherer, A. Yariv, J. D. OÕ Brien, P. D. Dapkus, and I. Kim, "Two-dimensional photonic band-gap defect mode laser," **SCIENCE**, 284, 1819-1821 (1999)

[9] M. T Hill, “Status and prospects for metallic and plasmonic nano-lasers,” **J. Opt. Soc. Am. B**, 27, 11, 36-44(2010)

[10] S. A. Maier, “Effective mode volume of nanoscale plasmon cavities.” **Opt. Quant. Electron**, 38, 257–267 (2006).

[11] T. W. Ebbesen, H. J. Lezec, H. F. Ghaemi, T. Thio, and P. A. Wolff, “Extraordinary optical transmission through sub-wavelength hole arrays,” **NATURE**, 391, 12-14 (1998)

[12] Y. Yin, T. Qiu, J. Li, and P. Chub, “Plasmonic nano-lasers,” **Nano Energy**, 1, 25–41 (2012)

[13] K. A. Willets, R. P. Van Duyne “Localized surface plasmon resonance spectroscopy and sensing, ” **Annual Review of Physical Chemistry**, 58, 267-297 (2007)

[14] M. T. Hill, Y. S. Oei, B. Smalbrugge, Y. Zhu, T. De Vries, P. J. Van veldhoven, F. W. M. Van Otten, T. J. Eijkemans, J. P. Turkiewicz, H. De waardt, E. J. Geluk, S. H. Kwon, Y.H. Lee, R. Notzel and M. K. Smit, “Lasing in metallic-coated nanocavities,” **Nature Photonics**, 1, 589-594 (2007)

[15] M. T. Hill, M. Marell, E. S. P. Leong, B. Smalbrugge, Y. Zhu, M. Sun, P. J.V. Veldhoven, E. J. Geluk, F. Karouta, Y. S. Oei, R. N¨otzel, C.-Z. Ning, and M. K. Smit, “Lasing in metal-insulator-metal sub-wavelength plasmonic waveguides,” **Opt. Express**, 17, 11107-11112 (2009)

[16] M. J. H. Marell, B. Smalbrugge, E. J. Geluk, P. J. van Veldhoven, B. Barcones, B. Koopmans, R. Nötzel, M. K. Smit, and Martin T. Hill, "Plasmonic distributed feedback lasers at telecommunications wavelengths," **Opt. Express**, 19, 15109-15118 (2011)

[17] M. W. Kim and P. C. Ku, "The metal-clad semiconductor nanoring laser and its scaling properties," **Opt. Express**, 19, 3218-3225 (2011)

[18] M. W. Kim and P. C. Ku, "Lasing in a metal-clad microring resonator," **APPLIED PHYSICS LETTERS**, 98, 131107 (2011)

[19] M. W. Kim and P. C. Ku, "Semiconductor nanoring lasers," **APPLIED PHYSICS LETTERS**, 98, 201105 (2011)

[20] A. M. Lakhani, M. K. Kim, E. K. Lau, and M. C. Wu, "Plasmonic crystal defect nanolaser," **Opt. Express**, 19, 18237-18245 (2011)

[21] X. Yang, A. Ishikawa, X. Yin, and X. Zhang, "Hybrid photonic−plasmonic crystal nanocavities," **ACS Nano**, 5, 2831-2838 (2011)

[22] Y. G. Wang, C. C. Chen, C. H. Chiu, M. Y. Kuo, M. H. Shih, and H. C. Kuo, "Lasing in metal-coated GaN nanostripe at room temperature," **APPLIED PHYSICS LETTERS**, 98, 131110 (2011)

[23] Y. G. Wang, S. W. Chang, C. C. Chen, C. H. Chiu, M. Y. Kuo, M. H. Shih, and H. C. Kuo, “Room temperature lasing with high group index in metal-coated GaN nanoring,” **APPLIED PHYSICS LETTERS**, 99, 251111 (2011)

[24] J. F. hackelford, W. Alexander, “Materials science and engineering handbook third edition,” CRC Press (2001)

[25] S. Adachi, “Physical properties of III-V Semiconductor Compounds - InP, InAs, GaAs, GaP, InGaAs, and InGaAsP,” Wiley-Interscience publication (1992)

[26] http://www.engineeringtoolbox.com/air-properties-d_156.html

[27] F. Kreith, “The CRC handbook of thermal engineering,” CRC Press (2000)

[28] 陳國樑 “光子晶體雷射的熱性分析,” Master thesis, NTHU (2010)

[29] M. H. Shih, W. Kuang, T. Yang, M. Bagheri, Z. J. Wei, S. J. Choi, L. Lu, John D. O’Brien, Senior Member, IEEE, and P. Daniel Dapkus, “Experimental characterization of the optical loss of sapphire-bonded photonic crystal laser cavities,” **IEEE PHOTONICS TECHNOLOGY LETTERS**, 18, 3, 535-537 (2006)

[30] M. H. Shih, M. Bagheri, A. Mock, S. J. Choi, J. D. O’Brien, and P. D. Dapkus, “Identification of modes and single mode operation of sapphire-bonded photonic crystal lasers under continuous-wave room temperature operation,” **APPLIED PHYSICS LETTERS**, 90, 121116 (2007)

[31] M H Shih, Y. C. Yang, Y. C. Liu, Z. C. Chang, K. S. Hsu and M. C. Wu, “Room temperature continuous wave operation and characterization of photonic crystal nanolaser on a sapphire substrate,” **J. Phys. D: Appl. Phys.**, 42, 105113 (2009)

[32] M. J. Webber, “Handbook of optical materials, ” CRC Press (2003)

[33] A. R. Degheidy and E. B. Elkenany “Theoretical investigation of the energy gaps temperature dependence in zinc-blende GaP and InP semiconductors at normal pressure,” **The African Review of Physics**, 135-144 (2012)

[34] A. V. Krishnamoorthy, K. W. Goossen, L. M. F. Chirovsky, R. G. Rozier, P. Chandramani, W. S. Hobson, S. P. Hui, J. Lopata, J. A. Walker, and L. A. D’Asaro “16×16 VCSEL array flip-chip bonded to CMOS VLSI circuit,” **IEEE PHOTONICS TECHNOLOGY LETTERS**, 12, 8, 1077-1075 (2000)

Appendix

Using Continuous Wave Pumping Condition

Besides, we use continuous wave pumping condition to obtain thermal resistance. The lasing wavelength shifts with temperature variation is 0.048 nm / K for non-coating ring and 0.021 nm / K for gold-coating ring. The lasing wavelength shifts with pumping power variation is 0.142 nm / mW for non-coating ring and -0.029 nm / mW for gold-coating ring. Figure A-1 is lasing wavelength shifting with temperature and pumping power variation individually for non-coating ring, and figure A-2 is lasing wavelength shifting with temperature and pumping power variation individually for gold-coating ring. The thermal resistance is 3 K / mW for non-coating ring and 1.4 K / mW for gold-coating ring by continuous wave pumping. The thermal resistance compares measurement result with simulation result is shown in table A-1. The thermal property is obvious for gold-coating ring at CW pumping condition. It has low thermal resistance and high thermal conductivity when coating metal such as gold.

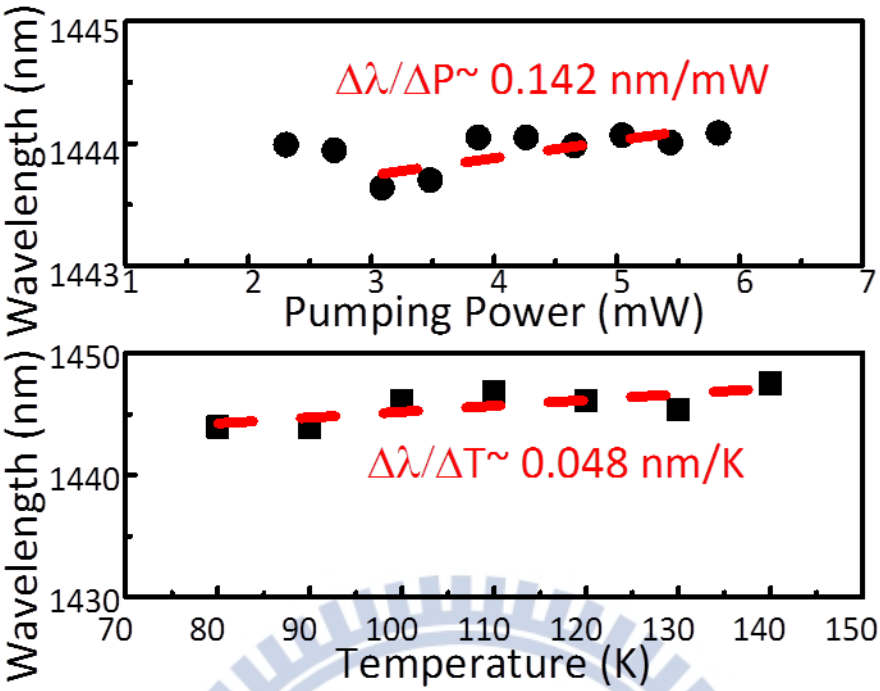

Figure A-1 The non-coating ring on sapphire. The $\Delta\lambda/\Delta T$ is 0.048 (nm/K), and the $\Delta\lambda/\Delta P$ is 0.142 (nm/mW).

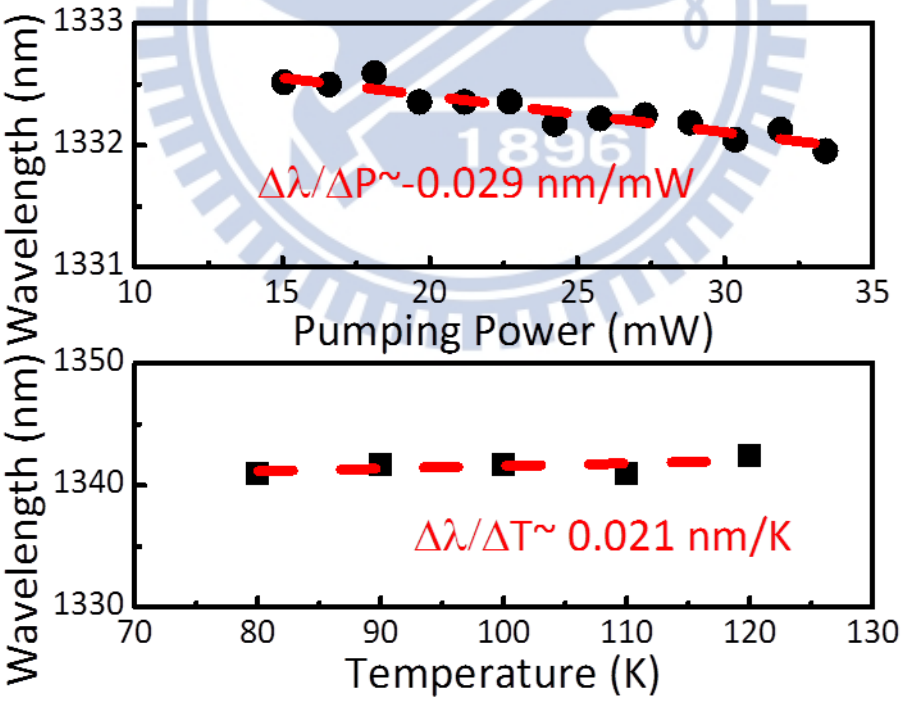

Figure A-2 The non-coating ring on sapphire. The $\Delta\lambda/\Delta T$ is 0.021 (nm/K), and the $\Delta\lambda/\Delta P$ is -0.029 (nm/mW).

Structure / Thermal resistance	Non-coating	Gold-coating	Ratio
Measurement (CW)	3 (K/mW)	1.4 (K/mW)	2.1
Simulation (CW)	80 (K/mW)	33 (K/mW)	2.4

Table A 1 The thermal resistance compares measurement with simulation at CW pumping condition.